Diurnal Variability in the Gate Region

By

Jean M. Dewart

P.I. William M. Gray

Department of Atmospheric Science
Colorado State University
Fort Collins, Colorado

NSF ATM 75-01424-A02

Colorado State University

Department of Atmospheric Science

Paper No. 298

DIURNAL VARIABILITY IN THE GATE REGION

By

Jean M. Dewart

Preparation of this report

has been financially supported by

National Science Foundation Grant No. ATM75-01424 A02

Department of Atmospheric Science

Colorado State University

Fort Collins, Colorado

November, 1978

Atmospheric Science Paper No. 298

ABSTRACT

This paper discusses the observational evidence for and the probable causes of the large diurnal variability of the atmosphere over the Inter Tropical Convergence Zone (ITCZ) region of the tropical eastern Atlantic Ocean. The analysis is based on the observational information of the A/B-scale rawinsonde data of the GARP[1] Atlantic Tropical Experiment (GATE).

A large single cycle diurnal oscillation of wind divergence similar to that observed in the western Atlantic and western Pacific oceans is found. Maximum divergences occur in the late morning, minimum in the early evening. Boundary layer divergence profiles show almost identical divergence for both convectively enhanced and convectively suppressed conditions. Tropospheric diurnal temperature variation is also investigated.

Vertically integrated radiational cooling values (Q_R) are evaluated as a residual from moisture and energy budget analysis. Applicability for the GATE ITCZ region of the Gray and Jacobson (1977) cloud and cloud-free diurnal radiational-convective forcing hypothesis is investigated. Energy budgets appear to diagnose physically realistic radiational differences between the convectively enhanced and suppressed cases. Moisture budgets indicate that the GATE rainfall maximum occurs in the late morning and that radar derived rainfall rates underestimate precipitation for the entire experiment by about $\sim$ 30-40%. Diurnal energy budgets are computed level by level in the vertical with the aid of a special assumption on condensation and evaporation in the vertical. Results are compared with the recent Phase III estimates of Cox and Griffith (1978).

The diurnal convergence cycle of the GATE A/B-array region appears to result from ITCZ vs. surrounding region north to south radiation differences. These diurnal radiational differences are enhanced by the presence of oceanic stratus and airborn Saharan dust to the north. There appears to be a substantial diurnal pulsing of the low level mass convergence into the GATE ITCZ region, particularly from the ITCZ's north side.

[1] Global Atmospheric Research Program.

TABLE OF CONTENTS

	Page
ABSTRACT	ii
1. INTRODUCTION	1
2. METHOD	9
2.1 Data	9
2.2 Moisture and Energy Budgets	12
3. RESULTS	14
3.1 Divergence Profiles	14
3.2 Diurnal Temperature Changes	24
3.3 Vertically Integrated Budget Computations	28
3.4 Vertical Resolution of Q_R	43
4. DISCUSSION	57
ACKNOWLEDGEMENTS	62
BIBLIOGRAPHY	63
APPENDIX A	66
APPENDIX B	68

1. INTRODUCTION

The diurnal variation of oceanic tropical weather systems has been a subject of much uncertainty. This diurnal variation has generally been thought to be small because the boundary layer over the oceans does not experience a large diurnal temperature cycle; and lapse rate stability does not vary diurnally as it does over land. However, Ruprecht and Gray (1976), Gray and Jacobson (1977) and McBride and Gray (1978) have recently documented a large diurnal variation in organized deep convection with a morning maximum and an evening minimum.

Ruprecht and Gray studied the diurnal variability of rainfall associated with cloud clusters in the Northwestern Pacific during the summers of 1967 and 1968 and also the diurnal variation of hourly precipitation from 13 years of rainfall data from 8 West Pacific stations. A striking (70% vs. 30%) diurnal cycle was observed in the heavy convective showers with morning amounts (07-12 Local Time - LT) being two and one-half times greater than early evening (19-24 LT) amounts. Cloud cluster tropospheric diurnal divergence profiles also indicated a much larger morning convergence from the surface to 400 mb (Fig. 1). This supports well the morning rainfall maxima.

Other rainfall and mass budget studies (McBride and Gray, 1978) have shown that this unexpected single cycle oscillation of tropical weather systems is present in the West Atlantic as well.

What is the cause of these diurnal variations? Gray (1976) has proposed that the deep convergence profile observed in tropical weather systems is maintained and diurnally modified by differences in the radiative-condensation heating profiles of the thick cirrus-shield

covered weather systems and their surrounding clear areas.

Specifically, the upper layered clouds of organized weather systems are largely opaque to IR energy. They prevent upward IR energy losses from lower layers and prevent a net flux divergence of IR energy in the layers underneath the cloud tops. In addition, condensation and evaporation resulting from upward vertical motion slightly warm the upper troposphere and cool the lower troposphere of the typical tropical weather system. By contrast, the upper levels of the surrounding cloud-free regions are not able to inhibit IR energy losses from lower layers. Cloud-free areas radiatively cool through IR energy loss at rates significantly greater than that at the same level of the disturbance underneath the cloud shield. The solar absorption of energy is also greatly altered by the presence or absence of cloud shields. Solar energy acts to increase the temperature of the cloud-free areas throughout the troposphere, but in disturbance regions with thick layered clouds it acts primarily to raise the temperature within the upper cloud decks. At the same time the surrounding clear or partly cloudy regions do not undergo significant temperature change from condensation and evaporation.

The heat balance is thus quite different in the two regions. In the cloud free area surrounding the cluster, the thermodynamic equation may be written as

$$\frac{\partial T}{\partial t} + \underset{\sim}{V} \cdot \underset{\sim}{\nabla} T + \omega (\Gamma_a - \Gamma_d) = Q_R \qquad (1)$$

Local Change of Temperature	Horizontal Advection	Subsidence Warming	Radiative Cooling

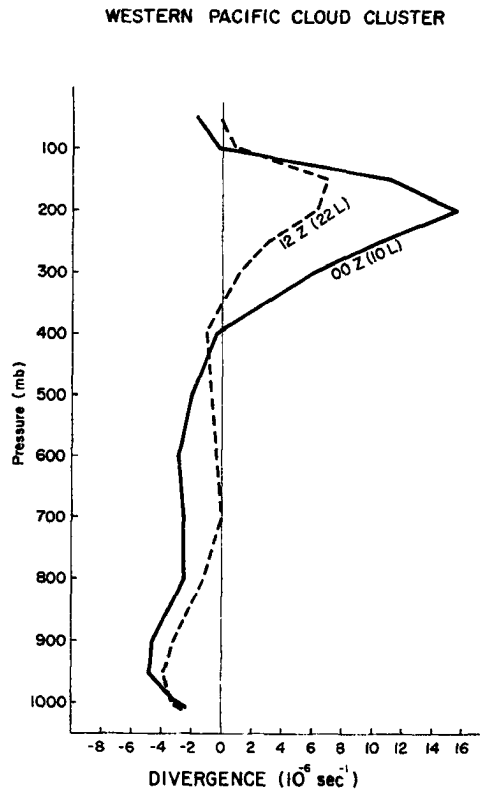

Fig. 1. Composited morning vs. evening cloud cluster divergence profiles (Ruprecht and Gray, 1976) for the area within 3^{o} of the center of the cloud cluster.

where ω is the vertical p-velocity and Γ_d, Γ_a are the dry and actual lapse rates.

In the cloud cluster the heat balance is defined as

$$\frac{\partial T}{\partial t} + \underset{\sim}{V} \cdot \underset{\sim}{\nabla} T = Q_{dis} \tag{2}$$

where

$$Q_{dis} = Q_{Convection} + Q_R. \tag{3}$$

Figure 2a portrays our estimate of typical day and night rates of combined radiation and convection temperature change within the tropical weather system. Also shown is the surrounding cloud-free

area day and night radiational cooling. This figure was derived from empirical studies of observed temperature change and from discussions with S. Cox and from his groups' radiation studies (Cox, 1969a, b, 1971 a, b; Fleming and Cox, 1974; Albrecht and Cox, 1975; Cox and Griffith, 1978). The tropical disturbance's surrounding clear or partly cloudy regions radiatively lose about twice as much energy at night as during the day. This radiation (Q_R) is the only diabatic energy source of the surrounding region and is balanced by subsidence warming. In the weather system the situation is more complicated. Besides radiation, diabatic energy sources of condensation (c) and evaporation (e) are also acting. In conventional notation the convective heating rate, $Q_{Convection}$, is

$$Q_{Convection} = \bar{\omega} (\Gamma_d - \Gamma_a) - \frac{\partial \overline{\omega' T'}}{\partial p} + L(c-e). \qquad (4)$$

$\bar{\omega}$ is the vertical p-velocity averaged over the scale at which measurements are taken, and ω', T' are deviations of vertical velocity and temperature from the measurement scale average. In an active tropical weather system the terms on the right of Eq. 4 have no physical meaning since the upward motion is moist adiabatic, taking place in active cumulus clouds. Gray (1973) demonstrated that the actual vertical motion within an active convective disturbance consists of a very large magnitude sub-synoptic or local up- and down-circulation, which is not resolved by mean or synoptic scale flow patterns. Thus, there is no synoptic scale adiabatic cooling $\bar{\omega} (\Gamma_d - \Gamma_a)$ actually taking place. For this reason the local heat balance of the cluster has been written as in Eq. 2.

Observed temperature changes in tropical weather systems indicate that 24-h vertically integrated averages of Q_{dis} are about zero. $Q_{Convection}$ closely balances Q_R. In the surrounding clear regions, however, the radiational cooling (Q_R) is always negative. This causes heating rate differences between the disturbance and its surroundings which are about twice as large at night as during the day. These day vs. night diabatic forcing differences are believed responsible for the observed divergence differences.

It is proposed that the diurnally varying radiative-convection heating differences between disturbances and their surroundings cause changes in the inward-outward disturbance pressure gradients. Due to the low value of the Coriolis parameter at tropical latitudes, the divergent and rotational components of the wind field do not change concomitantly. The lack of close wind-pressure balance produces significant ageostrophic flow, which diurnally modulates the observed convergence fields.

It is observed that disturbance temperature varies very little as a function of the amount of cumulus convection. Convection causes small rises in the upper tropospheric temperature and small decreases in the lower tropospheric temperature. Day-night variations of disturbance radiation cause larger temperature variation than do diurnal variations in condensation. This is particularly true in the upper troposphere where solar absorption causes upper tropospheric warming and enhanced nighttime cooling in comparison with the disturbance surrounding region. This causes day vs. night differences in upper tropospheric Q_{dis} as indicated in Fig. 2a which are only very weakly a function of day-night differences in the disturbance convection.

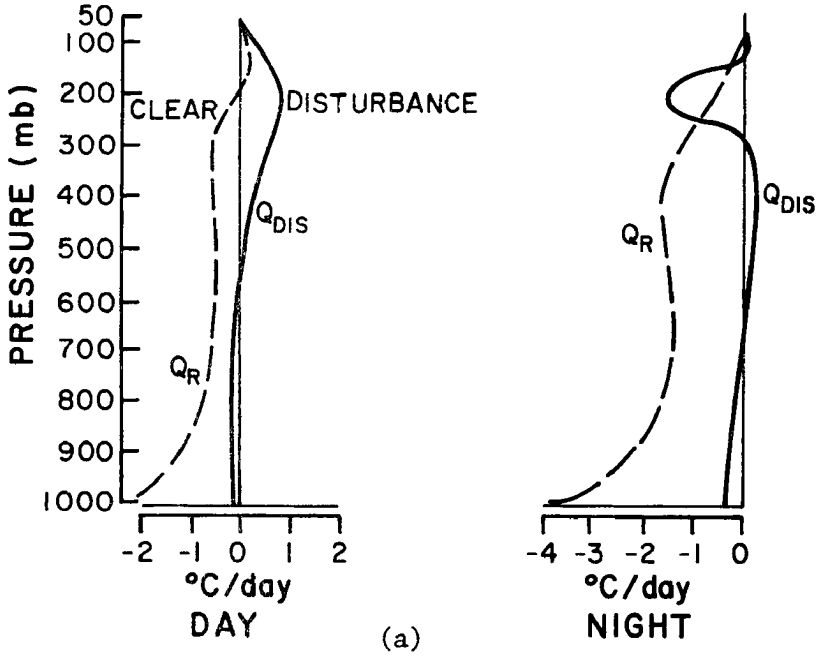

(a)

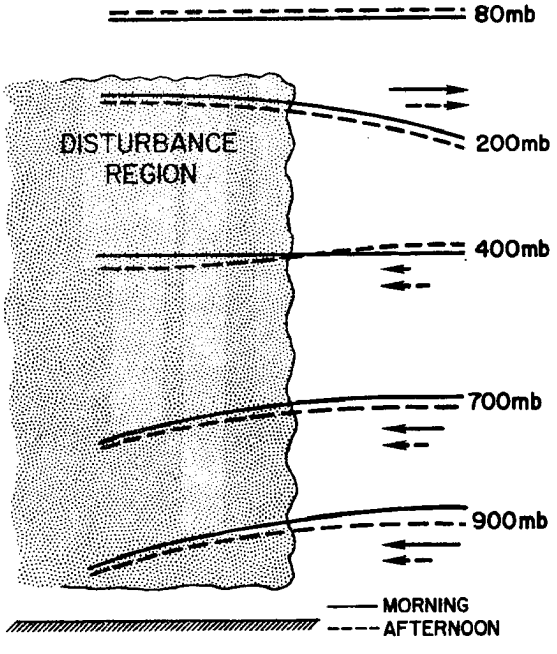

(b)

Fig. 2a-b. (a) Estimated typical day and night rates of radiation and condensation temperature change within a tropical disturbance and its surroundings. Q_{dis} represents the net radiative-convective heating rate in the disturbance (Eq. 2). Q_R is the net radiative heating rate in the surrounding clear or mostly clear region. (b) Slope of pressure surfaces forced by the heating differences in Fig. 2a. Lengths of the arrows are proportional to the strength of the mass circulation.

Thus, the disturbance minus surrounding region diabatic energy differences ($Q_{dis} - Q_R$) are largely driven by radiation and have a two to one night vs. day variation. This assessment has been well documented by the research project of W. M. Gray in reports by Jacobson and Gray (1976), Foltz (1976), Frank (1978), Grube (1978) and McBride and Gray (1978).

The atmosphere surrounding the organized tropical disturbance adjusts to its large radiational cooling at night through extra subsidence. This extra nighttime subsidence increases low-level convergence into the adjacent cloud regions. During the day solar heating reduces tropospheric radiation loss. Clear region subsidence warming and cloud region low-level convergence are substantially reduced.

At upper levels the cloud region cirrus shields radiationally cool more at night and less during the day than their surrounding cloud-free regions. This acts in a complementary fashion with conditions at lower levels to alter the cloud region and surrounding area pressure slopes and convergence profiles. This condition results in more convergence occurring in the morning and less in the afternoon-evening. The convergence cycle typically follows the radiational forcing with a time lag of 3-6h.

Figure 2b shows the hypothesized slope of pressure surfaces from the disturbance to its surroundings resulting from these radiational differences. Note that the daytime solar warming of the upper disturbance cloud layers produces an extra downward bulging of the middle tropospheric disturbance pressure surfaces in comparison with nighttime values. This causes an enhancement of the daytime middle-level convergence and a reduction at night. At lower levels the situation is reversed. Daytime solar warming of the region around the disturbance

causes a reduction of the low-level surrounding-disturbance pressure gradients and a consequent reduction of the daytime disturbance inflow as compared to the inflow at night.

This hypothesis has been extensively discussed in the reports of Gray and Jacobson (1977) and McBride and Gray (1978). Fingerhut (1978) has recently performed numerical experiments on a steady state tropical cloud cluster to test this radiation-convective hypothesis. The diurnal modulation of tropospheric radiation (shortwave plus longwave) profiles by a high cirrus layer was shown to produce day vs. night divergence profile differences similar to the observations. Tropospheric energy budget studies (Foltz, 1976) have also shown that the single cycle observed diurnal subsidence warming profile (morning maximum, evening minimum) is required to simultaneously balance the observed diurnal temperature changes with the expected radiational cooling profiles.

The present study was undertaken to further investigate the expected diurnal variations in the GATE region. The GARP Atlantic Tropical Experiment (GATE) has made available for the first time a large set of upper air observations that have made it possible to observe diurnal variations on a 3 to 6 hour basis. It also has a relatively long (60 days) duration of data collection. Thus, it is possible to more accurately describe the diurnal variability of the tropical atmosphere with the GATE data set than with any other previous information. In addition, the excellent spacial resolution of the GATE data has made it possible to further investigate the nature of these observed diurnal variations by computing diurnal moisture and energy budgets. From these budgets, radiational cooling profiles will be diagnosed as a residual in order to examine the relative role of radiation as a forcing mechanism for the diurnal oscillation of GATE region convergence.

TABLE 3

Suppressed Days

Julian Day	Date	A/B, B, C Rainfall	Number of Ships Reporting > Trace Rain
186	July 5	11 mm	2
190	July 9	24 mm	4
197	July 16	6 mm	3
216	Aug. 4	25 mm	7
226	Aug. 14	6 mm	4
227	Aug. 15	3 mm	2
243	Aug. 31	14 mm	5
244	Sept. 1	8 mm	4
250	Sept. 7	24 mm	9

In this study an alternative approach is taken. Instead of assuming the radiative cooling profile, it will be calculated as a residual. It is believed that the GATE A/B scale data has high enough time and spacial resolution to not only determine the large-scale heat and moisture sources, but also to allow an estimation of the partitioning of the condensation minus evaporation (c-e) term of the moisture budget in the vertical with a closure assumption of a simple cloud model. The radiative cooling term is then solved as a residual.

3. RESULTS

The diurnal variability of the GATE atmosphere is documented with vertical profiles of A/B scale divergences, B-scale temperatures, and A/B scale energy and moisture budgets. These diurnal changes are compared with oceanic tropical data from the Western Pacific and the Western Atlantic. Radiational cooling is calculated as a residual from the moisture and energy budgets. Calculations are compared with the radiation estimated by Cox and Griffith (1978) for Phase III.

3.1 Divergence Profiles

Average A/B scale divergence for the three GATE weather classes are presented in Fig. 4. The similarity of the GATE average and the enhanced cases indicates the convective character of the GATE A/B array within the ITCZ region. All three composites show low level convergence characteristic of a summertime ITCZ circulation. Above 850 mb, however, divergence of the GATE average and enhanced cases is quite different from the suppressed case.

The enhanced and GATE average cases show mid-level divergence between 800 and 400 mb. This divergence layer has appeared consistently in other GATE studies also, at the level of the low level easterly jet (Reed et al., 1977; Nitta, 1977). There is a shallow layer of convergence at 400 mb with the major outflow at 200 mb to 300 mb produced by the topping out of cumulonimbus towers.

The suppressed case also indicates mid-level divergence, from 900 mb to 400 mb. However, this layer has two peaks, one at 850 mb comprised of air from the boundary layer convergence, and one at 500 mb where air from the strong convergence aloft is diverging.

2. METHOD

2.1 Data

The internationally validated rawinsonde observations provided by CEDDA[2] (May, 1976) from the GATE A/B-scale and B-scale ships (Fig. 3) are the primary data source. Observations were taken at intervals of 3-6 hours during each of the three phases of GATE in the summer of 1974 off the west coast of Africa. These three phases are:

	Julian Date	Calendar Date
Phase I	179-197	June 28-July 16
Phase II	209-227	July 28-August 15
Phase III	242-262	August 30-September 19

Standard wind and thermodynamic observations are available every 5 mb in the vertical. CEDDA has flagged data from each sounding which appears to be in error. All such data have been discarded. Wind data have been averaged over 25 mb and the thermodynamic data have been used directly from the data tapes.

A number of problems with the rawinsonde data have been documented, however. These biases and inaccuracies are discussed more fully in Appendix A, but the two primary problems are the large amount of high frequency noise in the B-scale (U.S.) winds and the solar radiation correction applied to the USSR (A/B-scale) sonde measured temperatures. Due to the great sensitivity of the budgets to the wind field these problems have dictated that energy and moisture budgets be computed with A/B-scale winds only. Also, only B-scale temperature and humidity data will be used for the storage terms in the energy and moisture budgets.

[2]Center for Experiment Design and Data Analysis.

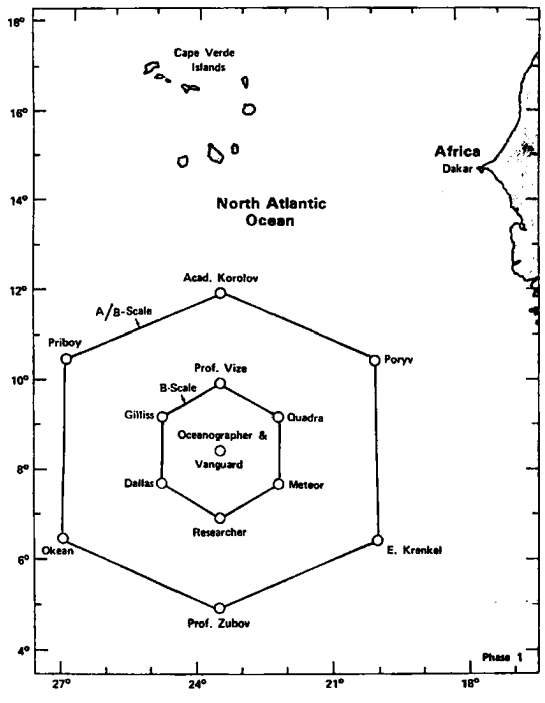

Fig. 3. The GATE ship array.

A composite rather than a case study approach has been chosen. A composite study can reveal the characteristics which are common to a number of meteorological conditions rather than individual case differences and can best isolate the true diurnal variations which are occurring. Data have been composited by ship position, and then averaged to form A/B-scale values. It has been verified that these results are the same as making calculations at individual times and then averaging.

Diurnal analyses have been made for three different GATE convective regimes. These are:

1) the GATE 60-day average,

2) ten of GATE's most convectively enhanced days, and

3) nine of GATE's most convectively suppressed days.

These are summarized in Table 1.

TABLE 1

Summary of Data Sets

1)	GATE Average:	All soundings from GATE composited by ship position.
	GATE Average Diurnal Case:	All soundings from GATE composited by individual time periods and by ship position.
2)	Suppressed and Enhanced Cases:	Selected individual days (data from 00Z-21Z on each day) composited to form an average, then recomposited into 0000, 0300, etc. time periods.

The GATE average case includes all soundings at 00 Greenwich Mean Time (Z), 06Z, 12Z and 18Z (these are 2230 LT, 0430 LT, 1030 LT and 1630 LT) from all three phases of GATE. The convectively enhanced case is composed of ten of the rainiest days in GATE (Table 2) as qualitatively determined by rainfall from all the ship gauges, satellite pictures and the B-array radar data. Visual radar data from the Oceanographer and Researcher were viewed to determine if the convection was approximately centered on the A/B-array. The convectively suppressed cases were determined in a similar manner (Table 3). Visual radar was again checked to determine whether the day was inactive or if the convection had just missed the ship rain gauges.

The enhanced and suppressed days are not purely enhanced or suppressed, however. Rarely is an entire day in the tropics convectively active as far as rainfall is concerned (Henry, 1974). But, so as not to bias the particular case towards any one time period, complete days from 00Z to 21Z were classified and composited for analysis.

TABLE 2

Enhanced Days

Julian Day	Date	A/B + B + C Ship Rain	A/B, B, C Ships w/over 50 mm rain/day
188	July 7	342 mm	Meteor (73 mm) Oceanographer (147 mm)
189	July 8	333 mm	Oceanographer (61 mm) Vanguard (58 mm) Researcher (122 mm)
195	July 14	305 mm	Poryv (78 mm) Gillis (52 mm)
222	Aug. 10	111 mm	Priboy (58 mm)
245	Sept. 2	252 mm	Planet (47 mm) Krenkel (64 mm)
248	Sept. 5	192 mm	Gillis (47 mm)
255	Sept. 12	278 mm	Dallas (98 mm) Fay (83 mm)
256	Sept. 13	450 mm	Quadra (107 mm) Okean (52 mm) Vanguard (66 mm) Dallas (71 mm) Fay (85 mm)
257	Sept. 14	322 mm	Meteor (68 mm)
259	Sept. 16	221 mm	Researcher (65 mm)

2.2 Moisture and Energy Budgets

The most popular method of determining the bulk thermodynamic effect of clouds on the large scale environment has been that of Yanai *et al.* (1973), where the large scale energy source and moisture sink is measured and then a cloud model is employed to determine the changes in energy and moisture due to cumulus entrainment, condensation, evaporation and detrainment. An assumed radiative cooling profile has been used in this approach.

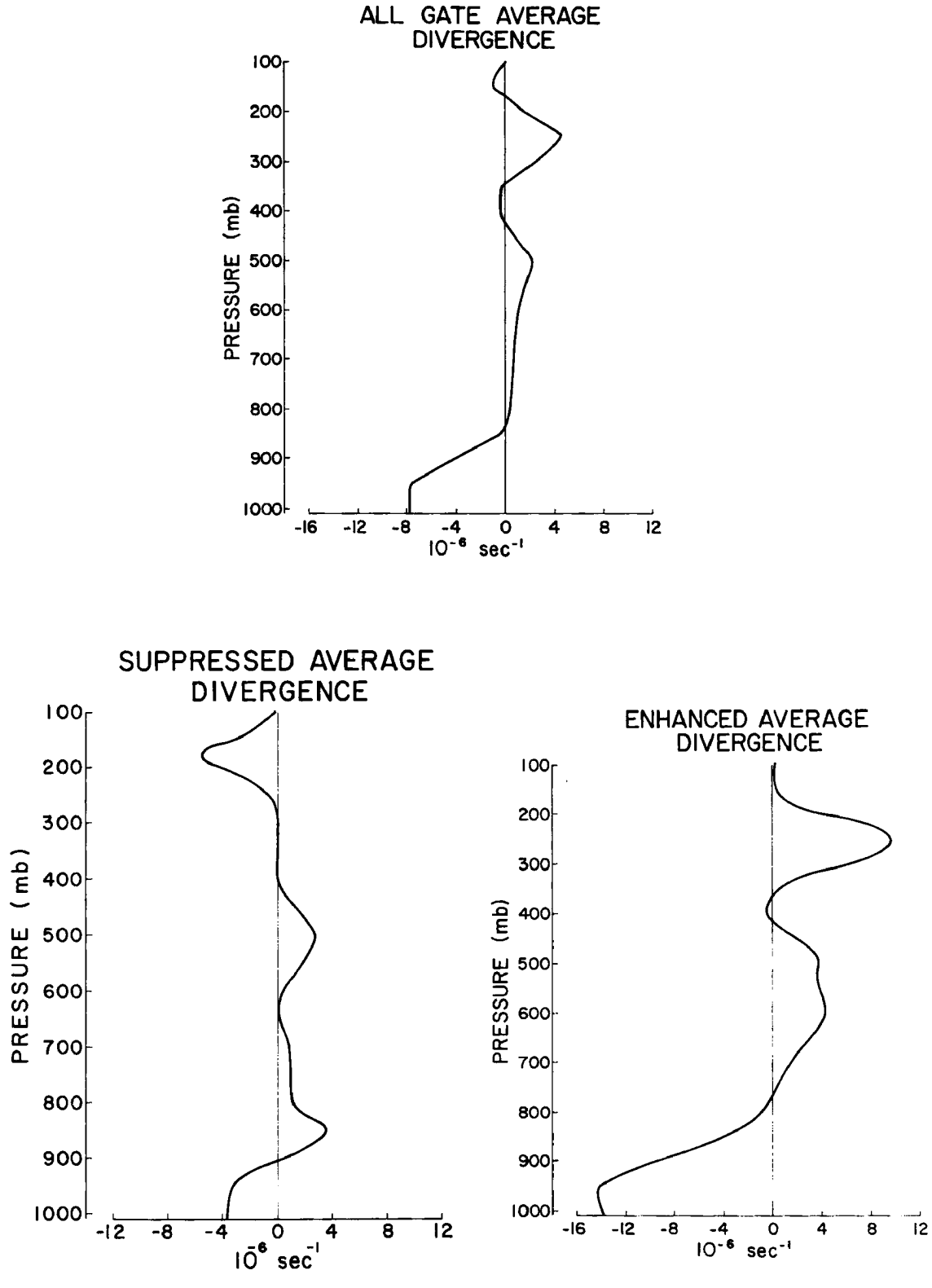

Fig. 4. A/B-scale divergence profiles for the all GATE average, suppressed average and enhanced average cases.

The GATE average and enhanced case divergence profiles show a large diurnal variation as indicated in Figs. 5 and 6. Note that:

1) Low level convergence follows a single cycle; maximum at 12Z minimum at 00Z.

2) Divergence from 500 mb to 300 mb is a maximum during the hours of greatest low level convergence, 06Z and 12Z.

3) From 350 mb to 450 mb convergence is present during the late afternoon and night while divergence is present in the early morning hours.

4) Upper level outflow is greatest and extends through the deepest layer in the late morning to late afternoon hours, 12Z to 18Z.

This cycle of divergence produces a large oscillation in the vertical motion profiles (Figs. 7 and 8). The maximum upward motion occurs in the early afternoon (15Z) and is twice the minimum value occurring at 00Z. The profiles indicate that while the low level convergence is a maximum between 0430 LT and 1030 LT (Figs. 5 and 6), large cumulonimbus clouds, as evidenced by large upper level vertical motion, do not respond until three to six hours later. Why the deep convection lags the low level convergence forcing will be discussed in conjunction with the moisture budgets.

Diurnally, the suppressed case (Fig. 9) has some similarities with the GATE average and enhanced case profiles. Low level convergence characteristic of the ITCZ region follows a single cycle and reaches a maximum at 1030 LT. Upward vertical motion of 40 mb/day occurs at 900 mb with upward motion extending to 250 mb. But while upper level subsidence is present only in the evening and night in the other two cases, subsidence is present at all times during the suppressed case (Fig. 10) with a progression as follows:

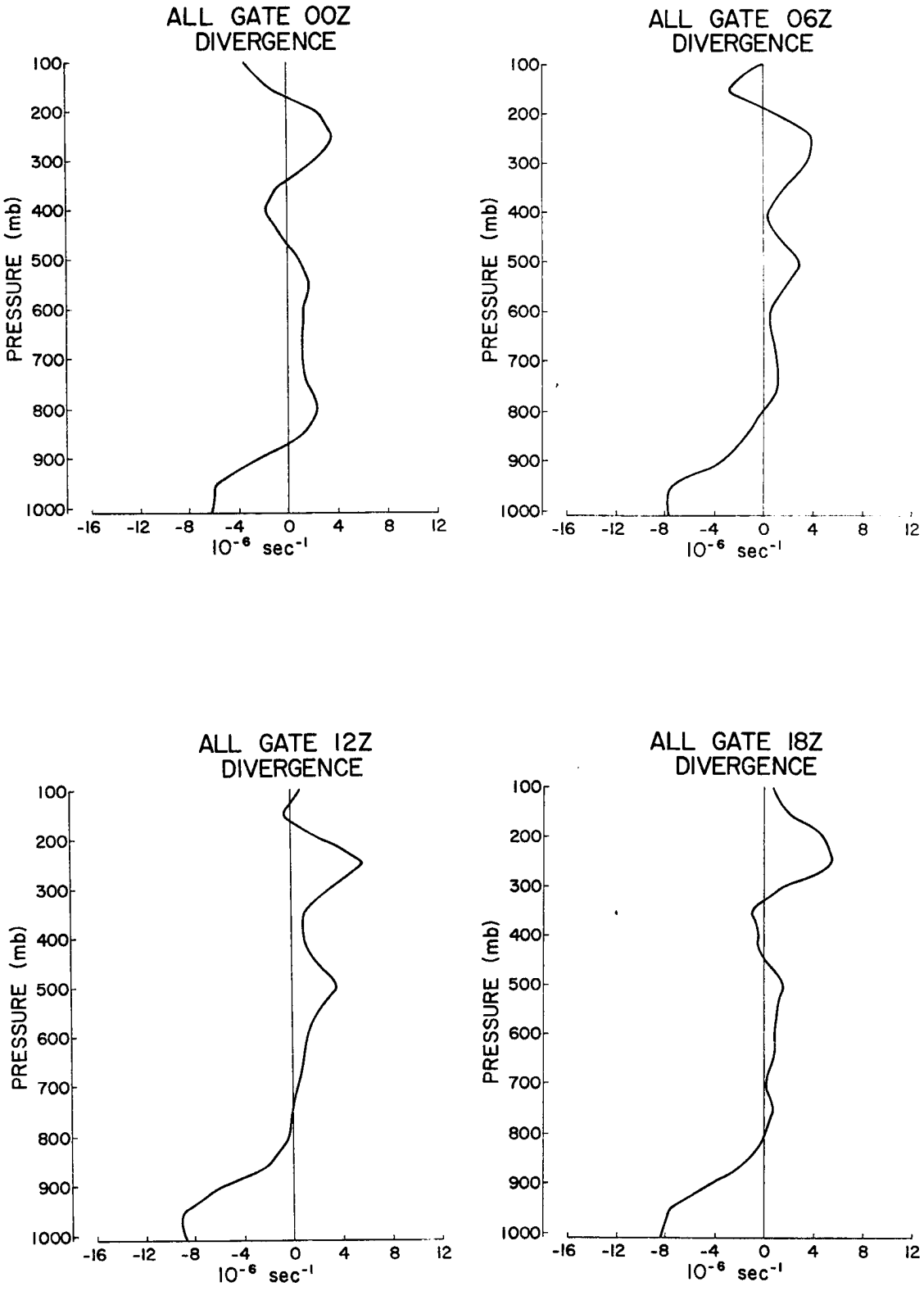

Fig. 5. Diurnal A/B-scale divergence profiles for the all GATE case. For local time subtract 1½ hours from Z time.

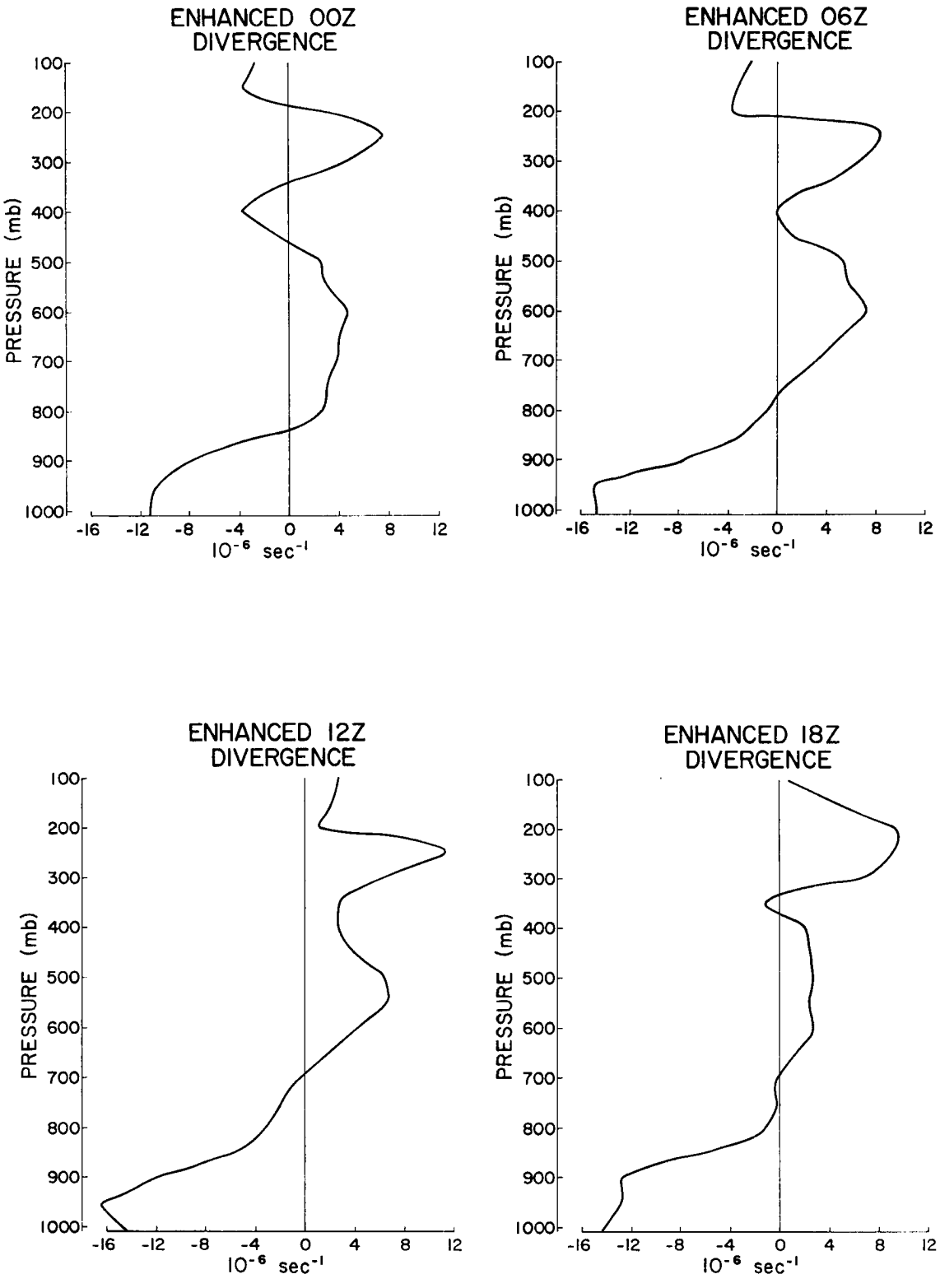

Fig. 6. Diurnal A/B-scale divergence profiles for the enhanced case. For local time subtract 1½ hours from Z time.

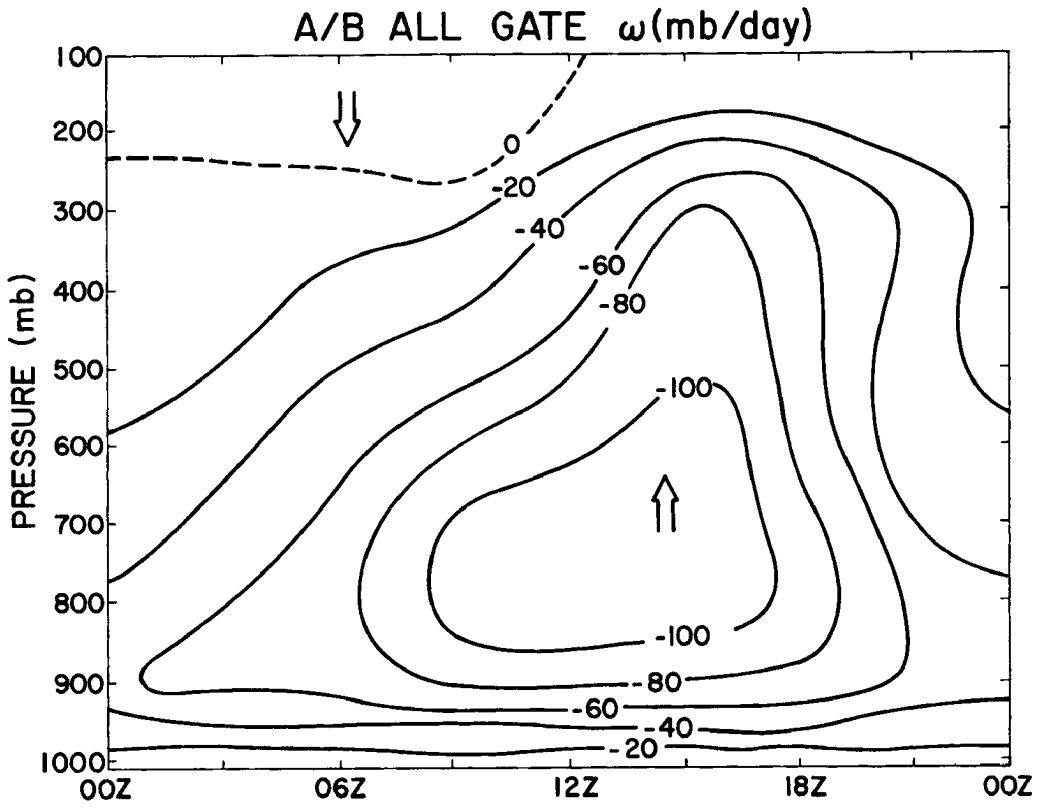

Fig. 7. Diurnal A/B-scale vertical motion for the all GATE case. For local time subtract 1½ hours from Z time.

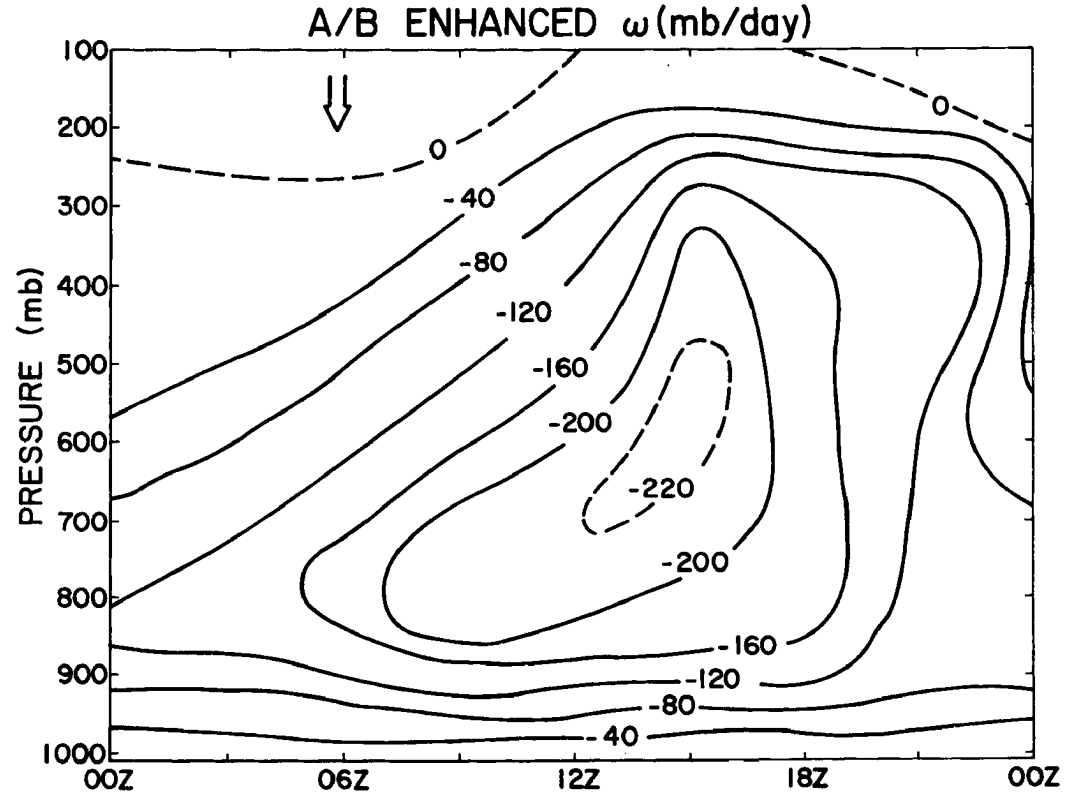

Fig. 8. Diurnal A/B-scale vertical motion for the enhanced case. For local time subtract 1½ hours from Z time.

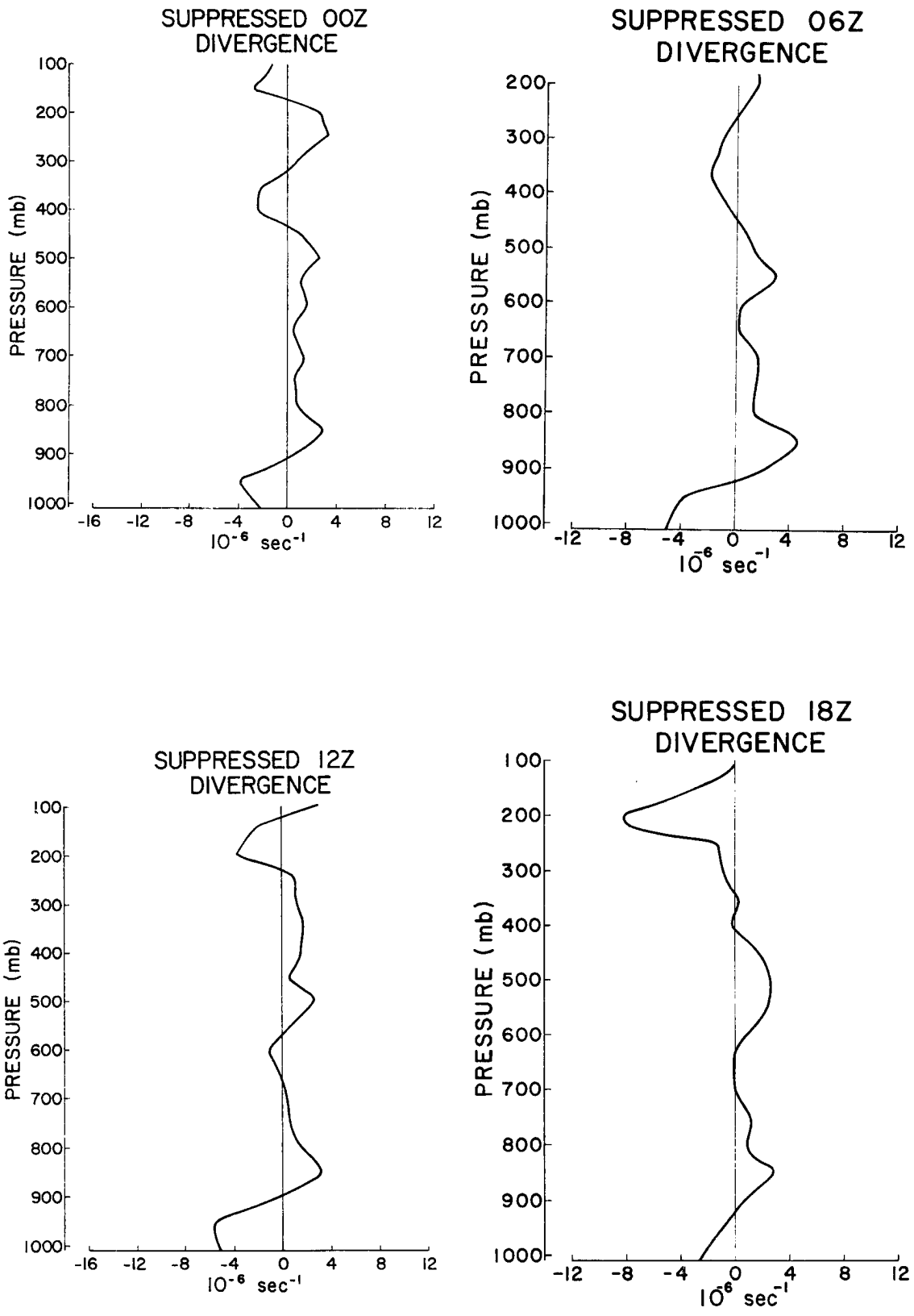

Fig. 9. Diurnal A/B-scale divergence profiles for the suppressed case. For local time subtract 1½ hours from Z time.

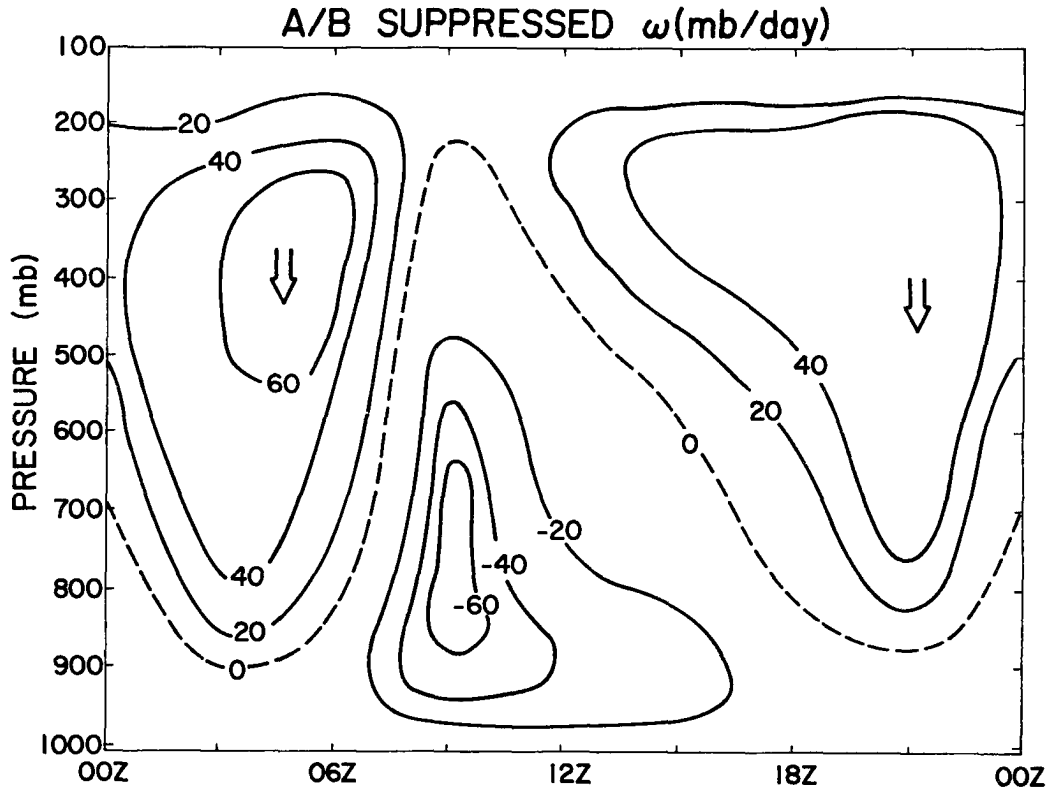

Fig. 10. Diurnal A/B-scale vertical motion for the suppressed case. For local time subtract 1½ hours from Z time.

1) Weakest subsidence is present in the morning during the time of greatest upward motion.

2) A deep layer of subsidence is established at 1630 LT.

3) A deep but weaker layer of subsidence continues into the nighttime.

4) Subsidence strengthens and extends through a deeper layer from 0130 LT to 0430 LT.

So, for the suppressed case, the upper layers appear to be responding to radiational forcing. Stronger nighttime radiative cooling in convectively suppressed regions than in enhanced regions will likely cause a stronger subsidence to occur by early morning in the suppressed regions such as has been numerically modeled by Fingerhut (1978) and such as is observed with the GATE suppressed cases. Such morning

subsidence maxima have also been measured at many global locations by Foltz (1976). The subsidence from 1630 LT to 1930 LT is likely a result of the return flow from the regions of enhanced convection. The suppressed case boundary layer, however, indicates the same diurnal forcing as the other two convective regimes. Convergence is always present with the maximum occurring in the morning, as with the enhanced and GATE average cases. This similarity of boundary layer diurnal convergence is an indication that the entire ITCZ region is diurnally pulsing. This diurnal pulsation within the GATE array occurs in conditions of both enhanced and suppressed convection.

As previously discussed, a similar cycle of diurnal divergence has been reported in other tropical oceanic regions. McBride and Gray (1978) have averaged wind reports around satellite tracked cloud clusters, pre-typhoon clusters, tropical storms and easterly waves which all show the morning maximum in low level convergence and upper level outflow (Fig. 11a-b). The GATE region is thus not unique when the morning vs. nighttime divergence profiles of convectively enhanced regions are examined. But the increased time resolution of the GATE data indicates that the primary maximum in upper level outflow in GATE is during the early afternoon for the enhanced and all GATE average cases rather than in the morning as in these western ocean weather systems. This observation is consistent with GATE convective cloud cover studies (McGarry and Reed, 1978) and rainfall studies (Hudlow, 1977). These show that the time of maximum cirrus cloud coverage and rainfall is between 1300 LT and 1500 LT. So, while GATE does have the same strong single cycle oscillation of low level forcing, the deep convection is delayed a few hours when compared to other regions.

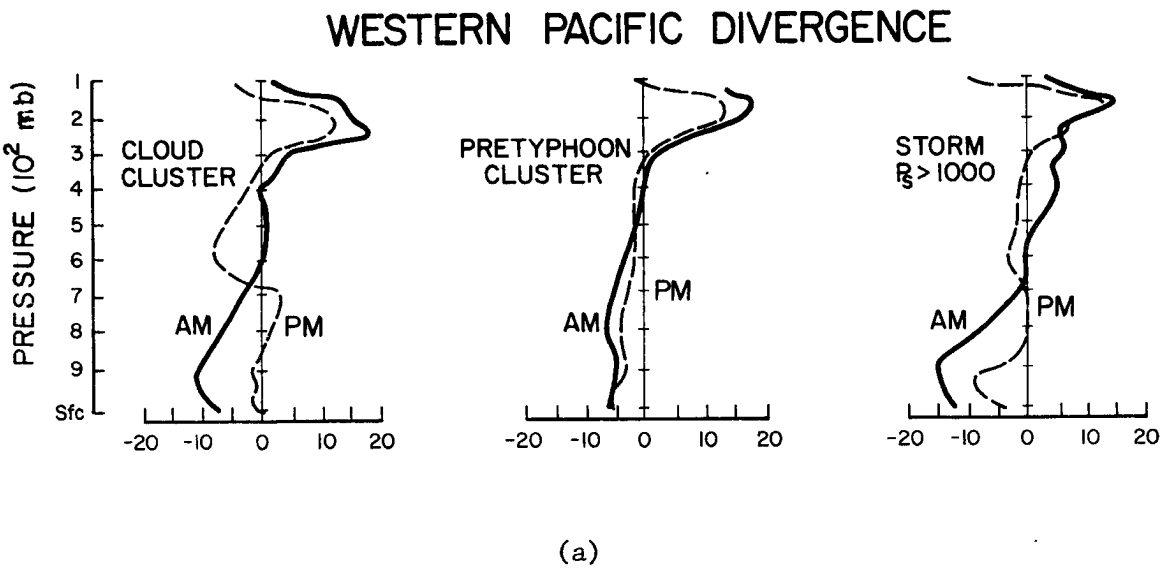

(a)

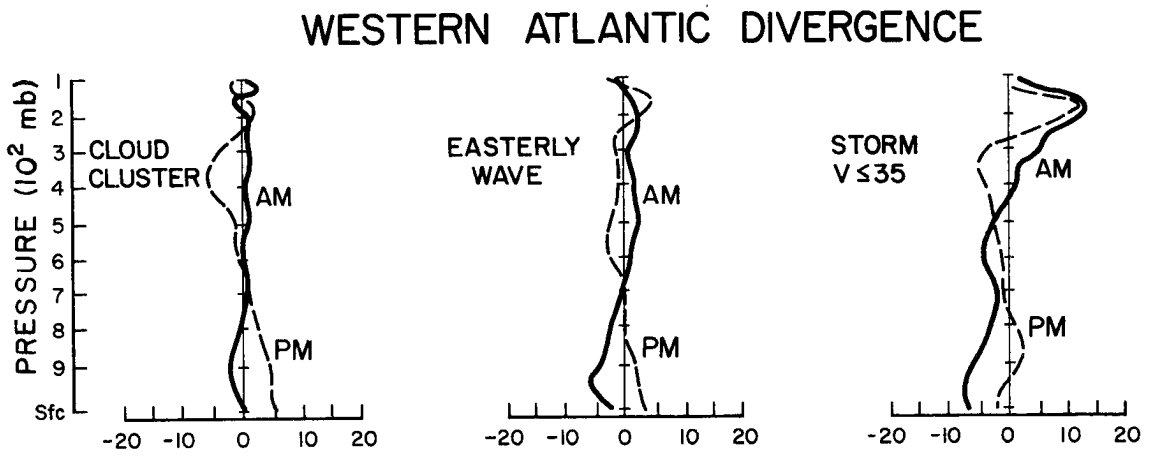

(b)

Fig. 11a-b. a) Morning vs. nighttime divergence profiles for Western Pacific cloud clusters, pretyphoon clusters, and tropical storms (from McBride and Gray, 1978). b) Morning vs. nighttime divergence profiles for Western Atlantic cloud clusters, easterly waves and tropical storms (from McBride and Gray, 1978).

The other difference between GATE and the western oceanic regions is the presence of a diurnal cycle of low level forcing in the GATE suppressed case, similar to the enhanced case. This has not been observed in the West Pacific as seen in Fig. 12, or West Atlantic areas where more low level subsidence occurs in the morning. As was earlier noted, this seems to indicate that the entire low level monsoon trough circulation is pulsing diurnally and independent of the amount of rain falling. This pulsing has also been documented by McBride and Gray (1978) when they analyzed the diurnal variability of easterly waves in GATE. Although there is upward motion throughout most of the atmosphere in the GATE wave ridges (Fig. 13), the boundary layer has a diurnal oscillation similar to that of the suppressed cases. Frictionally induced convergence cannot force this diurnal oscillation, as GATE boundary layer vorticity is much smaller than the convergence, and it does not reach a maximum until 9 to 12 hours after the convergence (Table 4). Indeed, the boundary layer convergence and vorticity are even out of phase with each other. Thus, frictionally induced convergence cannot explain the magnitude of the observed divergence or the observed diurnal cycle.

3.2 Diurnal Temperature Changes

The diurnal range of layer average temperatures in GATE is portrayed in Fig. 14. The dominant feature in each curve is the rise in temperature before short wave radiational heating is present or very strong. In this respect, GATE is like other oceanic tropical regions. Foltz (1976) has also documented a consistent rise in column averaged temperatures in the morning hours that could not be accounted for by radiation processes. Foltz hypothesized that in order to account for the observed temperature changes enhanced morning subsidence must be

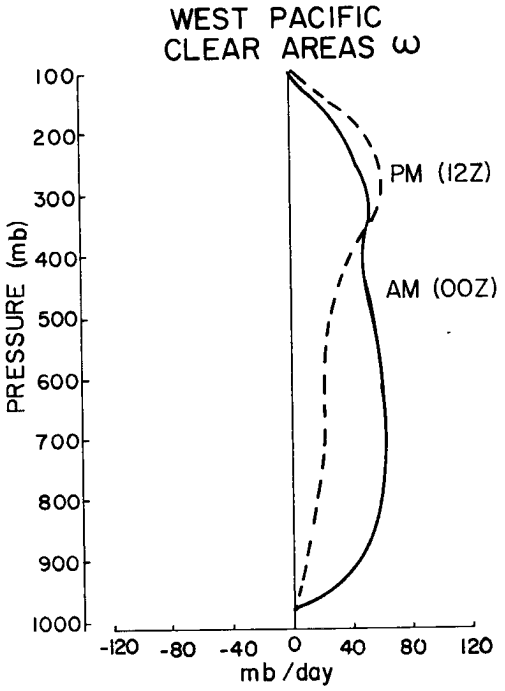

Fig. 12. Morning vs. nighttime vertical motion profiles for Western Pacific clear areas (from McBride and Gray, 1978).

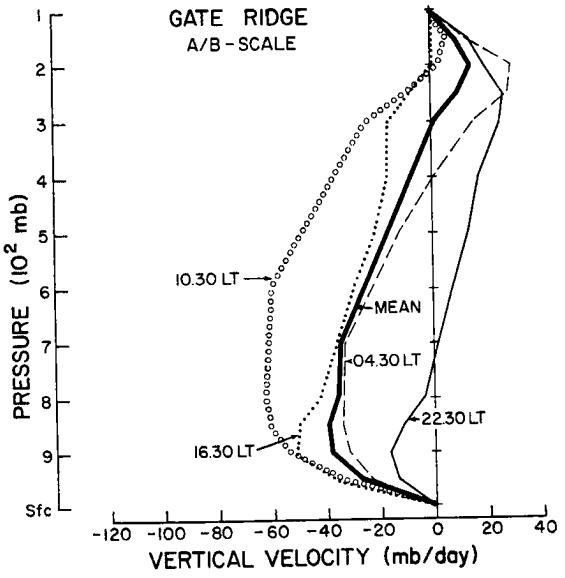

Fig. 13. Diurnal A/B-vertical motion profiles for GATE easterly wave ridge (McBride and Gray, 1978).

TABLE 4

Diurnal 900 mb divergence vs. vorticity (10^{-6} sec^{-1}) enhanced average case.

	00Z	03Z	06Z	09Z	12Z	15Z	18Z	21Z
Divergence	-8.0	-7.9	-7.6	-12.1	-11.9	-10.8	-2.7	-6.4
Vorticity	-1.2	-2.2	0	1.5	4.5	2.2	6.4	10.7

occurring. Since the warming rates he observed leveled off in the early afternoon, it appears that tropospheric subsidence must also have a diurnal cycle, i.e. large in the morning hours and small in the afternoon and early evening. Thus, at night the troposphere appears to cool to a point where a subsidence response sets in. The tropospheric temperature then begins to increase before solar heating becomes a factor. These temperature and subsidence diurnal cycles are what is observed in GATE. Diurnal profiles of ω in the enhanced and suppressed cases (Figs. 8 and 10) indicate that subsidence is occurring in the early morning hours (03Z to 09Z) when the temperature is observed to rise. Note that this extra subsidence at night will be more pronounced in convectively suppressed areas due to the larger radiational cooling under a clear sky (Fleming and Cox, 1974). This should increase the mass convergence into a convectively enhanced region in the morning and produce a rainfall maximum at that time.

Thus, the diurnal cycle of temperature in the GATE region also appears to support the argument that diurnal radiational forcing is a dominant tropospheric driving mechanism.

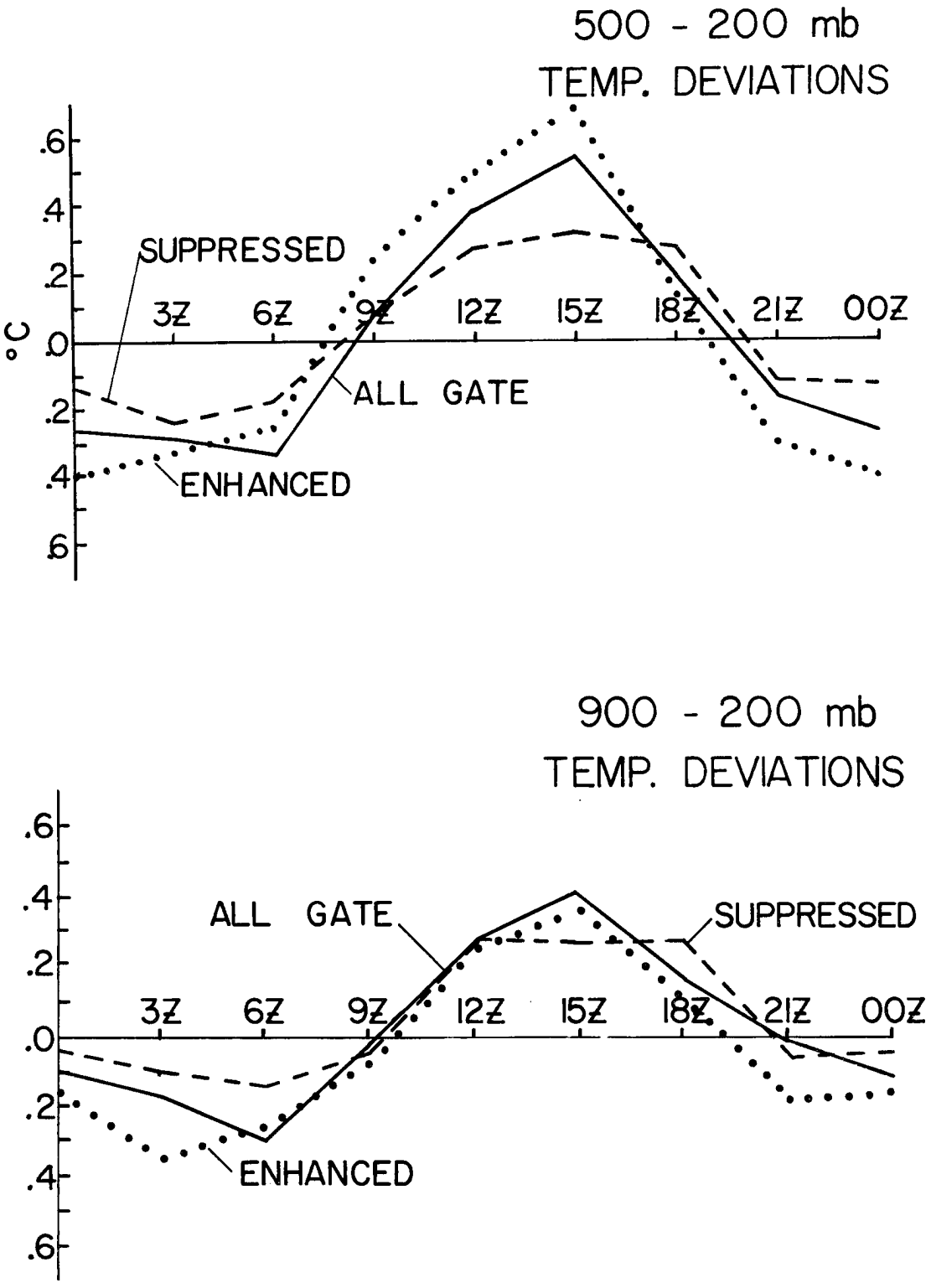

Fig. 14. Diurnal layer averaged temperature deviations from the mean temperature for the all GATE, enhanced and suppressed cases.

3.3 Vertically Integrated Budget Computations

Following Yanai et al. (1973) the equations for heat energy and moisture continuity for a large scale area, containing an ensemble of clouds which occupy only a fraction of the area are:

$$Q_1 = \frac{\partial \overline{s}}{\partial t} + \overline{\nabla \cdot s\underset{\sim}{V}} + \frac{\partial \overline{s}\,\overline{\omega}}{\partial p} = Q_R + L(c-e) - \frac{\partial}{\partial p}\overline{s'\omega'} \tag{5}$$

$$Q_2 = -L\left[\frac{\partial \overline{q}}{\partial t} + \overline{\nabla \cdot q\underset{\sim}{V}} + \frac{\partial \overline{q}\,\overline{\omega}}{\partial p}\right] = L(c-e) + L\frac{\partial}{\partial p}\overline{q'\omega'} \tag{6}$$

where

Q_1	=	apparent heat source
Q_2	=	apparent moisture sink
s	=	dry static energy
q	=	specific humidity
Q_R	=	radiation heating rate
$\underset{\sim}{V}$	=	horizontal wind
ω	=	vertical p - velocity
L	=	latent heat of condensation
c	=	condensation rate per unit mass
e	=	evaporation rate per unit mass.

Averages are computed over the horizontal extent of the A/B-array and deviations are taken from this horizontal average. The terms on the left side of both Eqs. 5 and 6 are the local change (or storage) term, the total horizontal convergence term, and the mean vertical divergence term. The terms on the right side of Eq. 5 are the heating due to radiation, the release of latent heat by net condensation, and the vertical convergence of the vertical eddy transport of sensible heat. The right side of Eq. 6 is the measure of the apparent moisture sink consisting of the net condensation and vertical divergence of the vertical eddy transport of moisture.

When Eq. 5 and 6 are vertically integrated from the surface (p_s) to 100 mb they reduce to:

$$\frac{1}{g}\left[\int_{p_s}^{P_{100}} \frac{\partial}{\partial t}\overline{s}\, dp + \int_{p_s}^{P_{100}} \overline{\nabla \cdot s\underset{\sim}{V}}\, dp\right] = \int_{p_s}^{P_{100}} Q_R \frac{dp}{g} + LP_o + S_o \qquad (7)$$

(a) (b) (c) (d) (e)

$$-\frac{1}{g}\left[\int_{p_s}^{P_{100}} \frac{\partial \overline{q}}{\partial t} dp + \int_{p_s}^{P_{100}} \overline{\nabla \cdot q\underset{\sim}{V}}\, dp\right] = P_o - E_o \qquad (8)$$

(a) (b) (c) (d)

L = latent heat of condensation

P_o = precipitation rate at the surface

E_o = evaporation rate at the surface

S_o = sensible heat flux from the surface (assumed to be 0.1 of E_o)

Computational Procedures. Computational procedures are as follows:

1) Terms (a) and (b) of Eq. 8 are directly determined from the GATE A/B-array rawinsonde data. Term (d) can be evaluated from the bulk-aerodynamic formula:

$$E_o = C_E \rho_o (q_s - q_a) |V_o| \qquad (9)$$

where $C_E = 1.3 \times 10^{-3}$

ρ_o = surface air density

q_s = saturation specific humidity at sea surface temperature

q_a = specific humidity 10 m level

$|V_o|$ = wind at 10 m level

P_o can thus be determined as a residual.

2) P_o can be substituted into term (d) of Eq. 7 and with the knowledge of terms (a) and (b) from the rawinsonde data, and term (e) from the assumption of the Bowen ratio (0.1), term (c), or the vertical integral of Q_R in Eq. 7 , can be solved as a residual.

Integrated A/B-Scale Moisture Budget. Integrated average moisture budgets are presented in Table 5. As expected the horizontal convergence term dominates, with the enhanced case having the largest convergence, 2.08 gm/cm^2 day. The evaporation rates are not greatly different between cases. The total amount of precipitation is sensitive to the storage term, but as discussed by Frank (1978) vapor storage is very small. Calculated drying of -0.13 gm/cm^2 day for the suppressed average and moistening of 0.32 gm/cm^2 day for the enhanced case may be too large due to small errors in vapor convergence. The all GATE A/B-array precipitation of 1.53 cm/day is 28% higher than Frank (1978) has estimated from s-budget calculations including Cox and Griffith's (1978) radiation estimation of 1.16^{o}C/day cooling (surface to 100 mb). Rainfall of 1.53 cm/day requires radiational cooling of 1.7^{o}C/day, 46% larger than Cox and Griffith's estimate. These differences will be discussed later. Despite an energy balance inconsistency, the diurnal range of values to be presented are believed to be

TABLE 5

A/B-Scale Moisture Budget (gm/cm^2 per day)

	$\overline{V_r q}$	E_o	$\partial q/\partial t$	P_o
ALL GATE	1.06	0.47	0.0	1.53
ENHANCED	2.08	0.49	0.32	2.25
SUPPRESSED	0.02	0.37	-.13	0.52

where $\overline{V_r q}$ = total moisture convergence

E_o = surface evaporation

$\partial q/\partial t$ = moisture storage

P_o = surface precipitation

TABLE 6

Moisture Budgets by Time of Day (gm/cm^2 per day)

	GMT	Local	$V_r q$	E_o	$\partial q/\partial t$	P_o
ALL GATE	00	2230	.59	.45	-.05	1.09
	06	0430	1.01	.47	-.21	1.69
	12	1030	1.41	.47	.05	1.83
	18	1630	1.19	.47	.21	1.45
ENHANCED	00	2230	1.32	.45	.25	1.52
	06	0430	1.84	.51	.20	2.15
	12	1030	2.61	.50	.60	2.51
	18	1630	2.36	.54	.20	2.70
SUPPRESSED	00	2230	.06	.38	-.11	.55
	06	0430	-.08	.35	-.53	.80
	12	1030	.37	.37	.01	.73
	18	1630	-.16	.36	.08	.12

approximately correct.

Diurnal moisture budgets are presented in Table 6. A large diurnal range in surface precipitation (P_o) is calculated. This is primarily produced by the diurnal cycle of horizontal moisture convergence, with the phase and amplitude of the oscillation somewhat modulated by the apparent moisture storage term. In each case, horizontal moisture convergence is greatest at 12Z (1030 LT) by a 2 to 1 margin over the minimum values at 00Z (2230 LT). This is not unexpected in light of the diurnal divergence profiles presented. The moisture storage term ($\partial q/\partial t$), if correct, slightly reduces the diurnal range of the P_o oscillation. It appears to play a significant role in modulating the phase of the oscillation, however. For instance, in the enhanced case the precipitation is larger at 18Z than at 12Z due to the apparent storage at 12Z. This delay in the precipitation maximum due to the storage term in the moisture budgets is difficult to accurately specify and have strong confidence in. But, these observations are consistent with the enhanced case divergence profiles which indicate a delay in the growth of large Cb's until the afternoon. The delay may be due to the large low level vertical wind shear found in GATE and the low level stability of the atmosphere. It takes a few hours longer (in comparison with other regions) for the cumulus convection in GATE to become organized into heavy rain producing Cb clouds. Moisture may be accumulating while this organization is occurring. Without storage, maximum rain in all regimes occurs at 12Z (1030 LT).

To determine the accuracy of these budget measurements, a number of other estimates are available for comparison; rain gauge data, radar reflectivity data, and satellite estimates. None of these measurements has an adequate spatial scale to resolve precipitation rates for

convectively suppressed conditions on the A/B-scale, however. No comparisons will consequently be made for the suppressed case.

Rain gauge estimates from the A/B and B-scale (Seguin and Sabol, 1976), B-scale radar-rainfall data (Hudlow, 1977) and B-scale radar data extended to the A/B-scale with satellite data (Hudlow, 1978[3]) are compared with the budget measured precipitation values in Table 7.

Good agreement is achieved concerning the phase of the diurnal cycle between the radar and budget values for the enhanced case. Both record a precipitation maximum from 12Z to 18Z and a minimum from 00Z to 06Z. A convective cloudiness study (McGarry and Reed, 1978) also concurs by documenting maximum area coverage during the early afternoon. But, for the all GATE case, the budget calculations indicate a morning maximum whereas, the gauge and B-scale radar data indicate an afternoon maximum.

There are also some discrepancies in the amount of precipitation recorded between the budget calculated precipitation rates and the other measurements. Undoubtedly, the gauge data underestimates the precipitation due to the lack of spatial resolution and ship structure interference, but the difference between the budget and radar-satellite estimates is not as easily reconciled. A/B-moisture budgets indicate $\sim$ 50 percent more rainfall (1.53 cm/day) than that indicated by the combined radar-satellite data (1.02 cm/day). In that the mean position of the ITCZ was centered on the B-array, one would expect the B-array to have significantly higher precipitation per unit area than the A/B-array due to its smaller areal extent. This occurs in the enhanced case, but not for the all-GATE case precipitation. The most likely explanation for this discrepancy rests with the possibility of the

[3]Personal communication.

TABLE 7

Comparison of GATE Precipitation Estimates (gm/cm^2 per day)

Data Source	A/B Budget This Study	% of Daily Total	B Radar Hudlow, 1978	% of Daily Total	A/B Satellite and Radar (Hudlow, 1978)	A/B, B, C Rain guage This study
ALL GATE AVE.	1.53		1.12		1.02	.85
00-06Z	1.39	23%	.88	20%		.62
06-12Z	1.76	29%	1.10	25%		.81
12-18Z	1.64	27%	1.40	31%		1.07
18-00Z	1.27	21%	1.09	24%		.89
ENHANCED AVE.	2.25		2.48			
00-06Z	1.84	20%	1.78	18%		
06-12Z	2.33	26%	2.31	23%		
12-18Z	2.61	30%	3.36	34%		
18-00Z	2.11	24%	2.47	25%		

radar estimates being more accurate for heavy convective showers and underestimating light and moderate precipitation. The other possibility is that the rawinsonde data are less accurate for the all-GATE than for the enhanced cases. This explanation can be ruled out by referring to the mass balance corrections applied to the two composites (see Appendix A). Both cases have had similar corrections made to the vertical wind profiles so that one cannot be said to have a more accurate divergence profile, and thus moisture budget, than the other. These small values of the A/B-scale radial wind (V_R) corrections attest to the excellent accuracy of the wind data. Also, in an individual time period study of GATE A/B-moisture budgets for all time periods, Frank (1978) who employed a least squares fitting technique to the winds to replace missing data, observed an all GATE P_o value of 1.36 gm/cm^2 per day. This value agrees within 13% with the budget values presented here. Thus, the budget calculated precipitation values are believed to be quite acceptable for all three convective regimes. As Frank (1978) has indicated and as previously discussed, these q-budget precipitation estimates may overestimate inward vapor transport by about 15% because they require a tropospheric radiational cooling of 1.7^{o}C/day which according to Cox and Griffith's estimates are too high. The reason for this is not fully understood at this time, but may be due to a mean dry advection across the GATE array which the Soviet ships cannot detect due to some systematic errors in their q measurement. Using Cox and Griffith's radiation estimates of -1.16^{o}C/day (surface to 100 mb) Frank calculates an A/B-array all-GATE rainfall of 1.20 cm/day. The Hudlow (1978) combined radar-satellite all-GATE rainfall estimate of 1.02 cm/day requires surface to 100 mb radiational cooling of only about -0.4^{o}C/day which is considered to be much too small.

There is some evidence to support the likely underestimate of lighter rain by the radar. Besides the consistency between the independent budget calculation of this study and Frank's (1978) study, data presented by Cunning and Sax (1977) indicate that the Z-R relationships used by CEDDA to transform the radar reflectivities to rainfall rates would underpredict the light and moderate rain showers in which 50% of the total rainfall in GATE fell (Gray and Jacobson, 1977). According to the Cunning and Sax data, rainfall rates of 7 mm/hr and 2 mm/hr are calculated as 6 mm/hr and 1 mm/hr respectively by CEDDA. This underestimation of light and moderate showers may also help explain the phase difference between the budgets and radar in determining the time of maximum rainfall for the all GATE case. The light and moderate showers must be occurring more in the morning for the all GATE budgets to give a morning maximum if the heavy showers occur in the afternoon. It is these lighter rainfall amounts which the radar is likely underestimating. This may cause the B-scale radar observed afternoon peak in rainfall for the all GATE case.

In this study, the budget derived precipitation estimates, although perhaps too high by 25% or so, will nevertheless still be used in the computation of radiational cooling. This overestimate of precipitation (if valid) should not significantly effect the determination of the diurnal cycle of the convective states which is the primary purpose of the paper.

Energy Budgets. To calculate residual values of radiational cooling, the precipitation rates (P_o) calculated from the moisture budgets are used in the energy budget equation (Eq. 5). When vertically integrated from the surface to 100 mb, the equation may be written as:

$$Q_1 - \overline{S}_o = \underset{(a)}{\frac{\partial \overline{s}}{\partial t}} + \underset{(b)}{\overline{\nabla \cdot s\underset{\sim}{V}}} = \underset{(c)}{\overline{L\,P_o}} + \underset{(d)}{\overline{Q_R}} \qquad (10)$$

Terms (a) and (b) are calculated from the rawinsonde data, term (c) from the moisture budget and term (d) is computed as a residual.

Vertically integrated values of this A/B energy budget are presented in Table 8. For the enhanced and suppressed average cases, general agreement is found between the budget calculated Q_R's and previously reported radiation profiles of Fleming and Cox (1974); and Albrecht and Cox (1975). Greater cooling is expected in the suppressed cases (-1.8^oC/day) than in the enhanced cases (-1.1^oC/day). This is presumably due to the reduction of IR energy loss by high clouds within the enhanced cases. Also during the daytime the enhanced case should warm in comparison to the suppressed case due to extra short wave absorption in clouds when compared with cloud-free conditions.

The all-GATE A/B-average of -1.7^oC/day appears to be somewhat larger than had been expected when the large amount of cloudiness in the GATE region (70%+, Holle et al., 1977) is considered. As the energy budget computation of Q_R is quite sensitive to the precipitation term ($L\,P_o$), a comparison of Q_R values diagnosed using different precipitation rates has been made for the all GATE case (Table 9). Of the three precipitation estimates, the Frank (1978) q-budget value gives the most physically realistic value of the all GATE Q_R when compared to the enhanced and suppressed average Q_R's. This may indicate that the budgets slightly overestimate the precipitation. It is clear, however, that the radar-satellite data significantly underestimates the radiational cooling obtained from those rainfall values.

TABLE 8

A/B Energy Budget (^{o}C/day)

	Q_1-S_o	L P_o	Q_R
ALL GATE	2.3	4.0	-1.7
ENHANCED	5.2	6.3	-1.1
SUPPRESSED	-.5	1.3	-1.8

TABLE 9

All GATE A/B Q_R as a function of L P_o

	P_o(gm/cm^{2}day)	L P_o(^{o}C/day)	Q_R(^{o}C/day)
A/B q-budget present study	1.53	4.0	-1.7
A/B q-budget Frank (1978)	1.36	3.6	-1.3
A/B s-budget with Cox and Griffith Phase III radiation	1.20	3.2	-1.16
Hudlow; A/B combined radar-satellite budget (1978)	1.02	2.7	-0.4

Cox and Griffith (1978) have derived Q_R profiles for Phase III using the radiative transfer equation with inputs of vertical temperature, moisture, and cloud top distribution. As Q_R's from Phase III are the only available values from Cox and Griffith (1978) the GATE average case will be compared with their Phase III average values.

The Cox and Griffith data from the days in Phase III which are included in this study's enhanced and suppressed cases will be compared to the budget derived enhanced and suppressed case Q_R values.

The Cox and Griffith data were presented in 4 six-hour averages for each day of Phase III (00-06 LT, 06-12 LT, 12-18 LT and 18-00 LT). As the budget data are presented for 00, 06, 12 and 18, the Cox and Griffith data were modified to produce averages at these times. Basically, the shortwave values for a six-hour period were adapted with a sine curve to give a representative value at 12Z or 18Z. The equations used for each time period are listed below:

Cox and Griffith LT Q_R to GMT Q_R

BUDGET		LW	SW
Q_R (00Z)	=	.75 LW(18-00) + .25 LW(00-06)	
Q_R (06Z)	=	.75 LW(00-06) + .25 LW(06-12)	+ .08 SW(06-12)
Q_R (12Z)	=	.75 LW(06-12) + .25 LW(12-18)	+ .92 SW(06-12) + .38 SW(12-18)
Q_R (18Z)	=	.75 LW(12-18) + .25 LW(18-00)	+ .62 SW(12-18)

The Cox and Griffith Q_R values for the average case are compared with the budget values in Table 10.

TABLE 10

A/B Q_R (^{o}C/day)

	Budget	Cox and Griffith (1978)
ALL GATE	-1.7	-1.2 Phase III only
ENHANCED	-1.1	-1.1
SUPPRESSED	-1.8	-1.2

Three points stand out in this comparison. First, there is good agreement between the two estimates of enhanced case cooling. This lends confidence to the magnitude of $-1.1^{o}C$/day for GATE convectively enhanced periods.

Secondly, there is a large disagreement between the all GATE budget calculated Q_R and the Cox and Griffith Phase III Q_R. The Cox and Griffith value is not large enough to balance the precipitation term in the heat budget equation.

The third result of the comparison is the lack of any difference between the enhanced and suppressed cases in the Cox and Griffith data. This is primarily due to a lack of substantial cloud differences between Cox and Griffith's Phase III enhanced and suppressed cases. Cox and Griffith have yet to make Phase I and Phase II calculations. When considering the high moisture content of the atmosphere in Phase III (5.1 cm of precipitable water) and the cloud top distributions (Table 11) it can be seen that Phase III is quite cloudy even on the days that very little rainfall occurs. Estimated Q_R's of this paper are believed more representative of suppressed conditions than Cox and Griffith's values because of the inclusion of Phase I and Phase II data. The budget determined suppressed case value of $-1.8^{o}C$/day also agrees quite well with the Fleming and Cox (1974) tropical clear sky estimates.

Diurnal budget calculated Q_R's are presented in Table 12. A relatively smooth diurnal cycle of Q_R's is diagnosed at each time period. This energy budget approach produces quite reasonable day vs. night radiational cooling differences. Each 00Z Q_R shows significantly greater cooling than 12Z Q_R's. The budget calculated Q_R's appear to

TABLE 11

Mean A/B Cloud Top Area Distribution (Cox and Griffith, 1978)

P(mb)	ENHANCED	SUPPRESSED
100	9.3%	1.4%
200	12.9%	3.8%
300	10.8%	4.6%
400	12.3%	7.4%
500	11.7%	13.1%
600	10.5%	13.3%
700	8.9%	11.7%
800	7.6%	10.4%
900	7.6%	13.1%
1000		
TOTAL	91.6%	78.8%

TABLE 12

A/B Energy Budget (^{o}C/day)

	Q_1-S_o	$L P_o$	Q_R	Night Average Q_R	Day Average Q_R
ALL GATE					
00 Z	.2	2.9	-2.7	} -2.5	
06 Z	2.4	4.7	-2.3		
12 Z	4.1	5.1	-1.0		} -1.3
18 Z	2.5	4.0	-1.5		
ENHANCED					
00 Z	1.7	4.3	-2.6	} -2.2	
06 Z	4.1	6.0	-1.9		
12 Z	7.7	7.0	.7		} 0
18 Z	6.7	7.5	-.8		
SUPPRESSED					
00 Z	-.5	1.4	-1.9	} -2.3	
06 Z	-.5	2.2	-2.7		
12 Z	1.0	1.9	-.9		} -1.4
18 Z	-1.5	.3	-1.8		

also yield physically realistic differences between the enhanced and suppressed cases. At each time period, except 00Z, the suppressed regime Q_R shows larger cooling than the enhanced. This is consistent with upper level cloudiness in the enhanced regions decreasing IR loss at night and increasing short wave absorption during the day to give the enhanced region a lower cooling rate.

There is one apparent inconsistency with the individual time period Q_R's, however. The enhanced vs. suppressed Q_R differences are larger during the day than at night. This is inconsistent with the previously discussed radiation hypothesis that requires that cloud-cloud free Q_R gradients be stronger at night (Fig. 2). The diurnal budget values are compared to the Cox and Griffith Q_R's in Table 13.

At any individual time period it can be seen that the two estimates differ by 0.1°C/day to 0.9°C/day, with the budget calculations

TABLE 13

A/B Q_R (°C/day)

	Budget	Cox and Griffith (1978)
ALL GATE		
00Z	-2.7	-1.8
06Z	-2.3	-1.7
12Z	-1.0	-.2
18Z	-1.5	-1.0
ENHANCED		
00Z	-2.6	-1.7
06Z	-1.9	-1.6
12Z	.7	-.2
18Z	-.8	-.9
SUPPRESSED		
00Z	-1.9	-1.9
06Z	-2.7	-1.8
12Z	-.9	-.1
18Z	-1.8	-1.0

usually giving more cooling. Day vs. night radiational cooling differences of $1^{o}C$/day to $2^{o}C$/day do compare however. Despite discrepancies between the absolute magnitudes of the two sets of Q_R's, they both produce similar day-night differences. However, it is important to note that even at individual time periods, Cox and Griffith's (1978) data do not show any differences between the enhanced and suppressed cases whereas the budget values show significant differences. This may partly be due to the lack of Phase I and Phase II data in the Cox and Griffith estimates.

3.4 Vertical Resolution of Q_R

For a more detailed study of the radiative term, an attempt was made to calculate its vertical distribution. The computational steps to accomplish this are as follows:

1) Determine terms on the left hand side of Eq. 6: $[-L\,(\frac{\partial \overline{q}}{\partial t} + \overline{\nabla \cdot q\underset{\sim}{V}} + \frac{\partial}{\partial p}\overline{q}\,\overline{\omega})]$ level by level from the A/B-array rawinsonde data. This is assumed to be the condensation resulting from the mean circulation.

2) Through special assumptions on the condensation-evaporation process determine the vertical distribution of Eq. 6 terms L(c-e) and $L\frac{\partial}{\partial p}\overline{q'\omega'}$ level by level.

3) Partition S_o in the vertical by assuming that all of the ocean sensible energy gain is realized in the boundary layer (surface to 950 mb).

4) After determining the terms on the left hand side of Eq. 5 from the A/B-array rawinsonde data, substitute at the individual levels the estimated values of (c-e) from Eq. 6 along with the S_o values from step 3) to obtain Q_R as a residual.

Computational steps 1, 3 and 4 are straightforward. Step 2 requires explanation. For step 2 a simple condensation-evaporation model is used to partition the L(c-e) and $\frac{\partial}{\partial p}\overline{q'\omega'}$ terms of Eq. 6 in the vertical. The L(c-e) term may be generally viewed as the net condensation resulting from the mean horizontal and vertical circulations through the system. The $\frac{\partial}{\partial p}\overline{q'\omega'}$ term should be primarily viewed as the upward vertical transport of water vapor from surface evaporation.

Specifically, this condensation-evaporation model is based on two assumptions:

A) the vertical distribution of the L(c-e) term in Eq. 6 is assumed to be given by the moisture accumulation due to the mean circulation or $[-L(\frac{\partial \bar{q}}{\partial t} + \overline{\nabla \cdot q\underset{\sim}{V}} + \frac{\partial\, \bar{q}\,\bar{\omega}}{\partial p})]$, and

B) the vertical distribution of the $L\,\frac{\partial\, \overline{q'\omega'}}{\partial p}$ terms is partitioned according to whether (c-e) in Step A is negative or positive. If this term is negative as occurs with subsidence, (c-e) is partitioned so that water vapor continuity is maintained. If this term is positive as with upward mean motion, the vertical partition of the vapor is made in proportion to the mean upward vapor transport.

From assumption A), for each 100 mb layer, from level 1 to 2 (except the surface to 950 mb layer) the moisture accumulation by the mean circulation is:

$$(c\text{-}e)_{1\text{-}2} = -\left[\frac{\partial \bar{q}}{\partial t} + \overline{\nabla \cdot q\underset{\sim}{V}} + \frac{\partial\, \bar{q}\,\bar{\omega}}{\partial p}\right]_{1\text{-}2} \qquad (11)$$

For the surface to 950 mb layer, which corresponds to the boundary layer, (c-e) is assumed to be zero. An example calculation is given:

	$\bar{\omega}$ mb/day	$\frac{\partial q}{\partial t}$ gm/cm^{2}day	$\overline{\nabla \cdot q\underset{\sim}{V}}$ gm/cm^{2}day	$\bar{\omega}\, q/g$ gm/cm^{2}day	$(c-e)_{1-2}$ gm/cm^{2}day
750	-38			.46 ↑	
		0	.12		.19
850	-54			.77 ↑	
		.01	-.30		.11
950	-34			.59 ↑	
		.01	-.51		0
SFC					
				E_o = .45 ↑	

The values of specific humidity used in the mean vertical divergence term are listed in Table 14. The mean q values are not used as water vapor is transported upwards in saturated cumulus updrafts and not with the mean synoptic scale ω. Water vapor is also transported downward by cumulus downdrafts and by mean compensating subsidence. So, the values for T_{up}, q_{up} and T_{down} and q_{down} are derived by estimating the temperature and moisture deviations of the upward and downward moving air parcels from the mean.

For assumption B) it must be noted that about $\sim$ 0.4 gm/cm^2 day is continuously accumulated in the oceanic tropical boundary layer due to evaporation. This vapor is continuously being transported out of the boundary layer by upward eddy flux processes of turbulence and cloud updrafts and downdrafts. The integrated vertical divergence of eddy moisture transport is set equal to this boundary layer excess and then partitioned in the vertical by the following procedure:

1) Determine the Boundary Lyaer Excess (BLE)

2) Sum up (c-e) due to large-scale vertical motion in the vertical in layers where (c-e) < 0. Define this as $(c-e)_{NEG}$.

3) Determine for each layer the ratio of the average vapor transport in that layer over the sum of the average vapor transport from all layers,

$$\left(\frac{\text{Vapor Transport}_{1-2}}{\text{Sum of all Vapor Transport}}\right).$$

Define this as % VT.

$$\% \text{ VT} = \frac{\overline{\omega q}_{1-2}}{g} \Big/ \sum_{p_s}^{p_{100}} \frac{\overline{\omega q}_{p_1-p_2}}{g}$$

4) Then,

$\frac{\partial}{\partial p} \overline{q'\omega'}_{1-2}$ (above 950 mb layer) is equal to

---

TABLE 14

Temperature deviations and specific humidities for vertical moisture budget calculations.

mb	T' (°C) up	T' (°C) down	q (gm/kg) q_{up}	q (gm/kg) q_{down}
150				
250	-.5	0	.4	.2
350	0	0	1.8	.9
450	.6	0	4.0	2.2
550	.8	-.1	6.3	3.9
650	.6	-.3	9.0	5.8
750	.4	-.5	11.8	7.9
850	.2	-.7	14.0	10.9
950	0	-1.0	17.1	13.7

$$\% \; VT_{1-2} [BLE + (c-e)_{NEG}] \quad \text{if } (c-e)_{1-2} > 0 \qquad \text{or}$$

$$\% \; VT_{1-2} [BLE + (c-e)_{NEG}] - (c-e)_{1-2} \quad \text{if } (c-e)_{1-2} < 0.$$

For example:

	$\overline{\nabla \cdot q\tilde{V}}$	$\frac{\partial q}{\partial t}$	$\frac{\overline{\omega q}}{g}$	(c-e)	% VT	$\frac{\overline{q'\omega'}}{g}$	$\frac{\partial}{\partial p}\overline{q'\omega'}$	Total (c-e)
650			.10↓					
	.08	-.16		.10	39%		.21	.31
750			.08↓			.20↑		
	.07	-.06		.11	26%		.14	.25
850			.04↑			.34↑		
	.04	.07		-.03	35%		.22	.19
950			.12↑			.56↑		
	-.38	.10		0				
SFC								
		E_o = .40↑						

where in this example:

$$BLE = .56 \text{ gm/cm}^2\text{day}$$

$$\sum_{p_s}^{p_{100}} \frac{\overline{\omega q}_{p_1-p_2}}{g} = .23 \text{ gm/cm}^2\text{day (when integrated through the troposphere)}$$

$$(c-e)_{NEG} = -.03 \text{ gm/cm}^2\text{day (when integrated through the troposphere)}$$

These procedures partition P_o in the vertical so that Q_R can be diagnosed as a residual level by level in the vertical. Many other assumptions concerning this partitioning could have been made, but in order to keep the calculations as simple as possible, this method was chosen.

Results of the vertical distribution of the mean moisture and energy budgets for the three basic convective regimes are presented in Tables 15, 16 and 17. Average radiative cooling profiles are shown in Fig. 15 along with comparable Q_R profiles from Cox and Griffith (1978). The budget calculated Q_R's have been smoothed in the vertical with a 1-2-1 binomial filter.

As Q_1 and L P_o are both a function of the vertical motion, the level by level budget calculated Q_R values are also a function of the vertical motion profile. In the all GATE case and the enhanced case (Fig. 15) the cooling maximum occurs at 700 mb, corresponding to the maximum in upward motion and precipitation production. For the suppressed case two maxima occur, one associated with the low level upward motion (900 mb) and one at 400 mb associated with the upper level sinking motion maximum.

In comparison, the Cox and Griffith (1978) curves (Fig. 15) are very uniform in the vertical without any pronounced maxima or minima above the lowest 50 mb. Their profiles reflect the very smooth distribution of cloud top heights used in their computations (Table 11). For the enhanced and all GATE budget, calculated Q_R is larger than the Cox and Griffith results below 500 mb and smaller above. For the suppressed case, the budget results agree fairly well except in the upper troposphere.

TABLE 15

A/B All GATE Average Moisture and Heat Budget

PRESSURE (10^2mb)	mb/d $\bar{\omega}$	gm/cm^{2}d $\overline{\nabla \cdot Vq}$	gm/cm^{2}d $\frac{\overline{\omega}\,\overline{q}}{g}$	gm/cm^{2}d $\frac{\partial q}{\partial t}$	gm/cm^{2}d (c-e)	gm/cm^{2}d $\frac{\overline{\omega' q'}}{g}$	gm/cm^{2}d $\frac{\partial}{\partial p}\frac{(\overline{\omega' q'})}{g}$	gm/cm^{2}d Total (c-e)	°C/d Total (c-e)	°C/d $Q_1 - S_o$	°C/d Q_R	°C/d Smoothed Q_R
-1		0		0	0			0	0	0		
-	-2		0									
-2		0		0	.01			.01	.2	-.5	-.7	-.7
-	-18		.01↑									
-3		0		0	.06		.01	.07	1.7	1.1	-.6	-.6
-	-39		.07↑			.01↑						
-4		-.01		0	.10		.01	.11	2.6	2.1	-.5	-.8
-	-40		.16↑			.02↑						
-5		.02		0	.18		.03	.21	5.0	3.2	-1.8	-1.7
-	-55		.36↑			.05↑						
-6		.04		0	.22		.05	.27	6.5	3.6	-2.9	-2.9
-	-67		.62↑			.10↑						
-7		.03		0	.25		.08	.33	6.0	3.6	-2.4	-2.7
-	-74		.90↑			.18↑						
-8		0		0	.20		.11	.31	7.4	4.4	-3.0	-2.7
-	-77		1.10↑			.29↑						
-9		-.49		0	.12		.10	.22	5.3	3.0	-2.3	-2.2
-	-42		.73↑			.39↑						
-10		-.65		0						-1.2	-1.2	-1.2
			E_o= .47 ↑									
TOTAL		-1.06		0	1.14		.39	1.53				-1.7

TABLE 16

A/B Enhanced Average Moisture and Heat Budget

PRESSURE (10^2mb)	mb/d $\bar{\omega}$	gm/cm^{2}d $\overline{\nabla \cdot \nabla q}$	gm/cm^{2}d $\frac{\bar{\omega}\,\bar{q}}{g}$	gm/cm^{2}d $\frac{\partial q}{\partial t}$	gm/cm^{2}d (c-e)	gm/cm^{2}d $\frac{\overline{\omega' q'}}{g}$	gm/cm^{2}d $\frac{\partial}{\partial p}\frac{(\overline{\omega' q'})}{g}$	gm/cm^{2}d Total (c-e)	°C/d Total (c-e)	°C/d $Q_1 - S_o$	°C/d Q_R	°C/d Smoothed Q_R
-1												
-2	-1	0	0	0	0			0	0	.8	.8	.8
-3	-37	0	.01↑	.01	.14			.14	3.4	3.4	0	.5
-4	-87	0	.16↑	.05	.16		.01	.17	4.1	5.4	1.3	.7
-5	-91	.06	.37↑	.08	.26	.01↑	.02	.28	6.7	6.8	.1	-.4
-6	-120	.12	.77↑	.09	.42	.03↑	.04	.46	11.0	7.9	-3.1	-2.7
-7	-153	.07	1.40↑	.08	.45	.07↑	.07	.52	12.5	7.8	-4.7	-3.5
-8	-166	-.18	2.0 ↑	.04	.35	.14↑	.09	.44	10.5	8.9	-1.6	-2.2
-9	-155	-1.01	2.21↑	-.03	.15	.23↑	.09	.24	5.8	4.8	-1.0	-1.4
-10	-75	-1.14	1.32↑	-.01		.32↑				-2.2	-2.2	-2.2
			E_o = .49 ↑									
TOTAL		-2.08		.31	1.93		.32	2.25				-1.1

TABLE 17

A/B Suppressed Average Moisture and Heat Budget

PRESSURE (10^2mb)	mb/d $\overline{\omega}$	gm/cm^{2}d $\overline{\nabla \cdot \nabla q}$	gm/cm^{2}d $\frac{\overline{\omega}\,\overline{q}}{g}$	gm/cm^{2}d $\frac{\partial q}{\partial t}$	gm/cm^{2}d (c-e)	gm/cm^{2}d $\frac{\overline{\omega' q'}}{g}$	gm/cm^{2}d $\frac{\partial}{\partial p}\frac{(\overline{\omega' q'})}{g}$	gm/cm^{2}d Total (c-e)	°C/d Total (c-e)	°C/d $Q_1 - S_o$	°C/d Q_R	°C/d Smoothed Q_R
-1												
	7		0			0						
-2		0		0	-.01		.01	.01	.2	-1.9	-2.1	-2.1
	36		.01↓			.02↑						
-3		0		-.01	-.01		.01	.01	.2	-1.8	-2.0	-2.1
	36		.03↓			.04↑						
-4		.01		-.03	-.03		.02	.02	.5	-2.0	-2.5	-2.4
	34		.08↓			.09↑						
-5		.04		-.04	.02	.12↑	.03	.05	1.2	-1.4	-2.6	-2.2
	15		.06↓									
-6		.04		-.05	.02	.14↑	.02	.04	1.0	-.2	-1.2	-1.5
	9		.05↓									
-7		.04		-.04	.03	.16↑	.02	.05	1.2	.4	-.8	-1.1
	3		.02↓									
-8		.21		-.02	.01	.26↑	.10	.11	2.6	.8	-1.8	-1.9
	-13		.18↑									
-9		-.03		.05	.09	.36↑	.10	.19	4.6	1.4	-3.2	-2.2
	-16		.29↑									
-10		-.29		.01						-.7	-.7	-.7
			$E_o = .37^{\uparrow}$									
TOTAL		.02		-.13	.12		.31	.52				-1.8

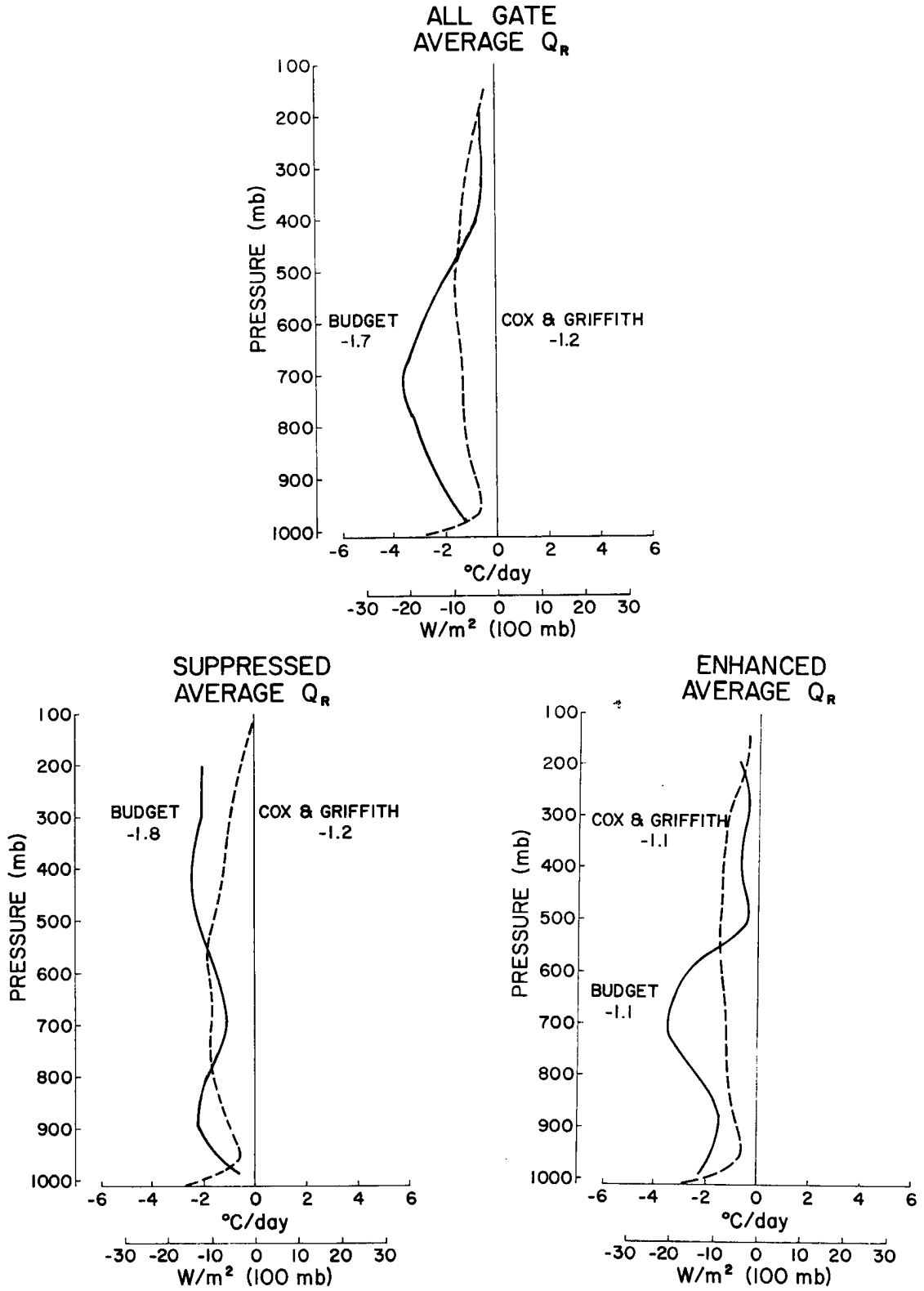

Fig. 15. Level by level budget calculated Q_R profiles for the all GATE, enhanced and suppressed average cases with comparative curves from Cox and Griffith (1978). The value listed on each curve is the vertically integrated Q_R for that curve in $^{o}C/day$. The lower abscissa units are Watts $\cdot$ m^{-2} $\cdot$ $(100\ mb)^{-1}$.

The level by level diurnal moisture budgets are presented in Appendix B for the three convective regimes. The Q_R profiles for each time period are presented in Figs. 16 to 18.

For each composite the level by level budget calculated Q_R's follow a smooth diurnal cycle similar to the vertically integrated Q_R's. This energy budget approach is also able to diagnose upper level radiational warming in the enhanced and GATE average case at 12Z. This is consistent with upper level clouds being warmed through shortwave absorption around noon. This does not occur in the suppressed case due to upper level sinking motion at 12Z. Physically, this sinking should reduce the amount of cloudiness at high levels and so reduce upper level shortwave absorption in comparison with the convectively enhanced case. Thus, although the budgets diagnose Q_R as a residual, they appear to give some results consistent with an idealized model of significant cloud-cloud free radiational differences.

A number of features in the budget calculated Q_R profiles are, however, inconsistent with the vertical distribution of Q_R previously hypothesized by various radiation modellers. Nevertheless, the ability of the diurnal energy and moisture budgets to diagnose a smooth and realistic diurnal oscillation of Q_R within each regime in the vertical is considered promising. It is encouraging that it may be possible to use the GATE data to solve for the vertical distribution of radiation.

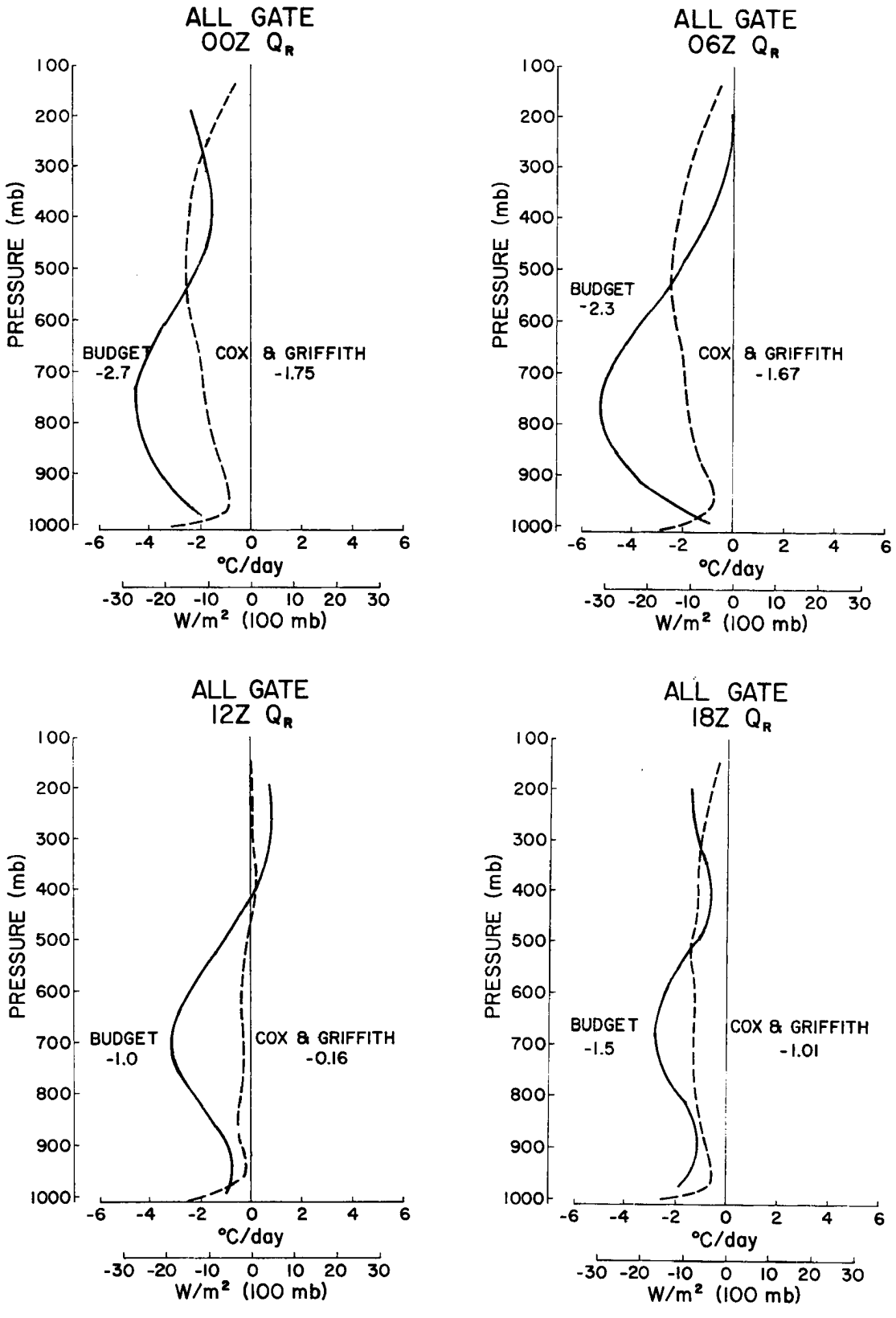

Fig. 16. Diurnal budget calculated Q_R profiles for the all GATE case. Cox and Griffith (1978) diurnal values for Phase III.

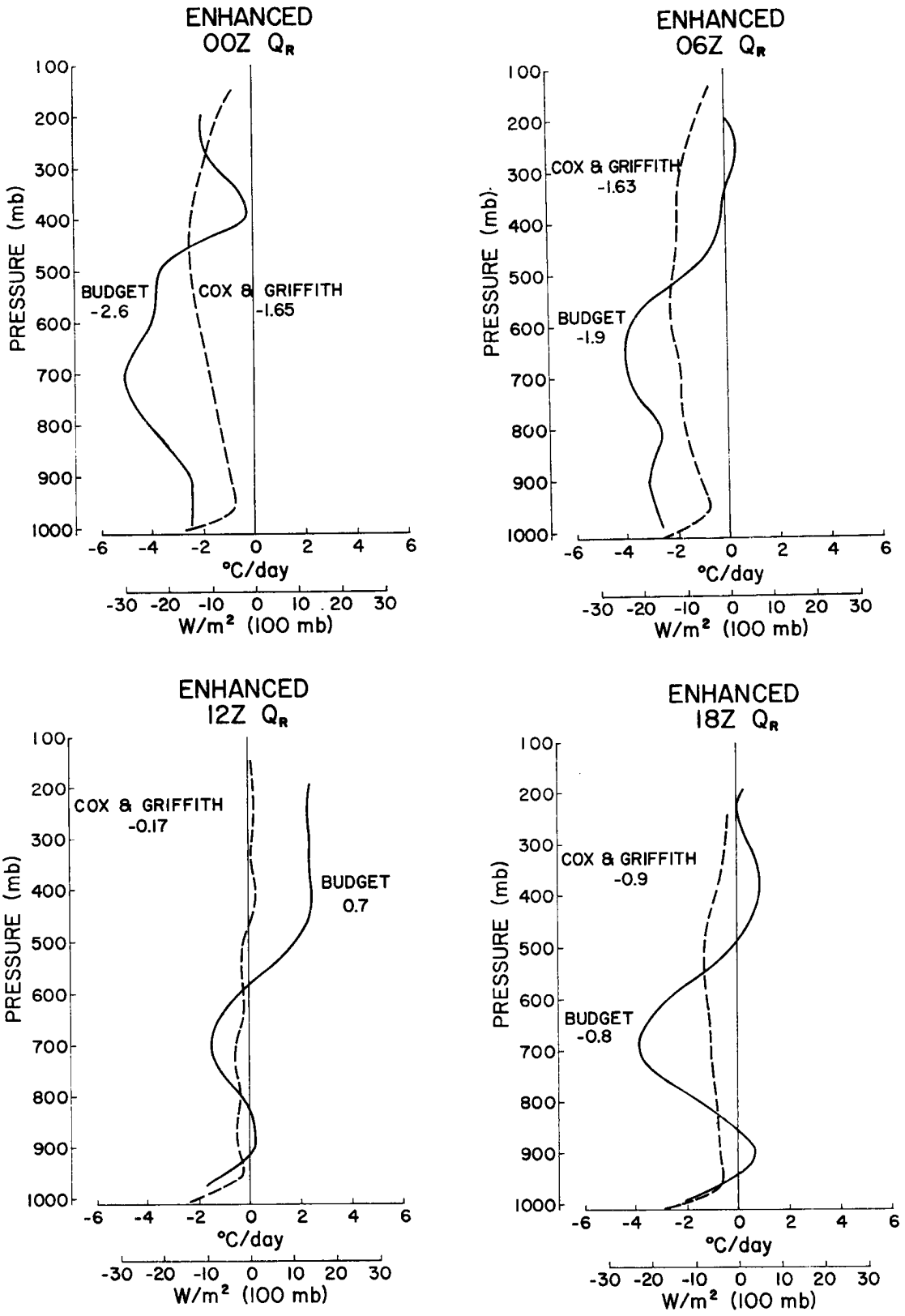

Fig. 17. Diurnal budget calculated Q_R profiles for the enhanced case. Cox and Griffith (1978) Q_R for enhanced case days from Phase III.

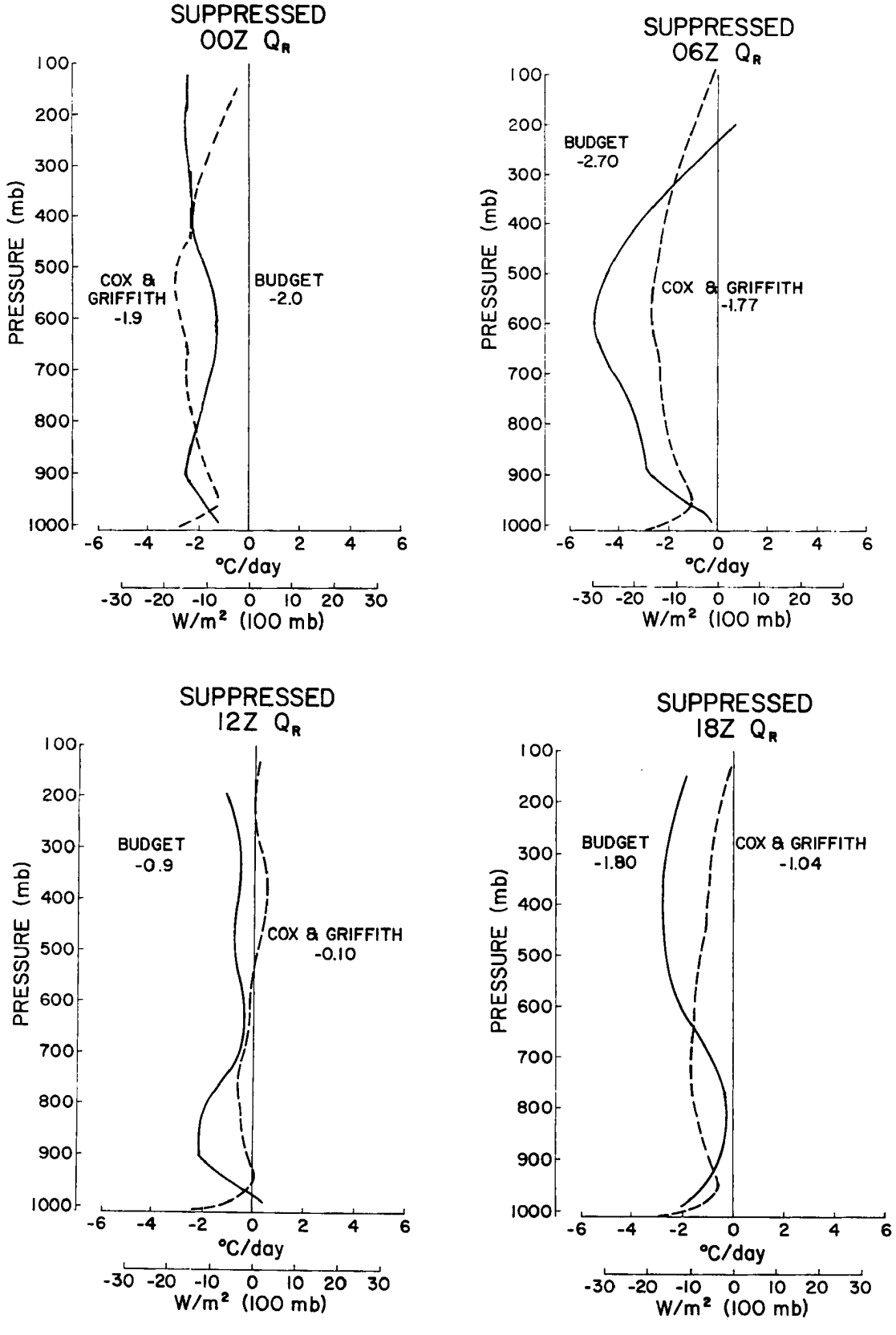

Fig. 18. Diurnal budget calculated Q_R profiles for the suppressed case. Cox and Griffith (1978) profiles for suppressed case days from Phase III.

4. DISCUSSION

This study shows that there exists a large single cycle oscillation of wind divergence profiles in the ITCZ region of the eastern Atlantic Ocean. This diurnal variation is similar to that previously found in the tropical western Atlantic and western Pacific by Ruprecht and Gray (1976), Gray and Jacobson (1977) and McBride and Gray (1978). A late morning maximum and evening minimum of low level convergence is observed. The moisture budget analysis for the entire experiment indicates a 0430 LT to 1030 LT maximum vs. a 1630 LT to 2230 LT minimum difference in precipitation of two to one. This is consistent with the divergence profiles. But, unlike the western ocean regions, the moisture budget analysis of convectively enhanced days in GATE indicates an early afternoon (1030 LT to 1630 LT) maximum in deep convection. This is probably due to the large low level vertical wind shear and greater lapse-rate stability of the GATE region which acts to delay the development of organized Cb cloud lines until a few hours after the maximum low level convergence. This time lag of convection is not as large in the western oceans.

The A/B moisture budget analysis indicates that the B-scale radar-rainfall measurements (Hudlow, 1977) likely underestimate the B-scale precipitation for the entire GATE period by as much as 30-40%, and the A/B-scale radar-satellite estimates (Hudlow, 1978[4]) appear also to underestimate rainfall by about 30-40%. These underestimates are thought to be caused by the radar's lack of resolution of light and moderate intensity rainfall.

---

[4]Personal communication.

The mechanism responsible for this large diurnal single cycle divergence oscillation is likely the day vs. nighttime differences in the gradients of radiative and convective heating between the convectively enhanced ITCZ region and the surrounding convectively suppressed regions to the north and south. These diurnal differences cause diurnal pressure gradient alterations which act to enhance the morning and suppress the evening low-level mass convergence in and out of the ITCZ region. As seen in Fig. 19 (Cox and Griffith, 1978) radiational cooling gradients between an active ITCZ and the convectively suppressed regions to the north and south are much stronger at night than during the day. This produces a stronger mass convergence into the low levels of the ITCZ in the early morning hours than in the evening, consistent with the observations. These cooling gradients are thought to occur on the scale of the Hadley Cell and appear to be primarily north-south as opposed to east-west differences. The diurnal radiation gradients between the GATE ITCZ and the oceanic area 10^{o} to 15^{o} to the north are unusually pronounced due to enhanced IR cooling from stratocumulus cloud decks at night and enhanced daytime solar absorption by Saharan dust (McBride and Gray, 1978).

The radiational character of the ITCZ was observed to be rather uniform in the east-west direction by Cox and Griffith with the diurnal oscillation of boundary layer convergence occurring all along the east-west extent of the ITCZ in both convectively enhanced and suppressed conditions. This diurnal ITCZ mass convergence is portrayed in idealized form in Figs. 20 and 21.

Diurnal energy budgets have been computed to derive an independent set of radiational cooling values (Q_R) for the GATE A/B-array for comparison with radiation values derived by Cox and Griffith (1978) for the

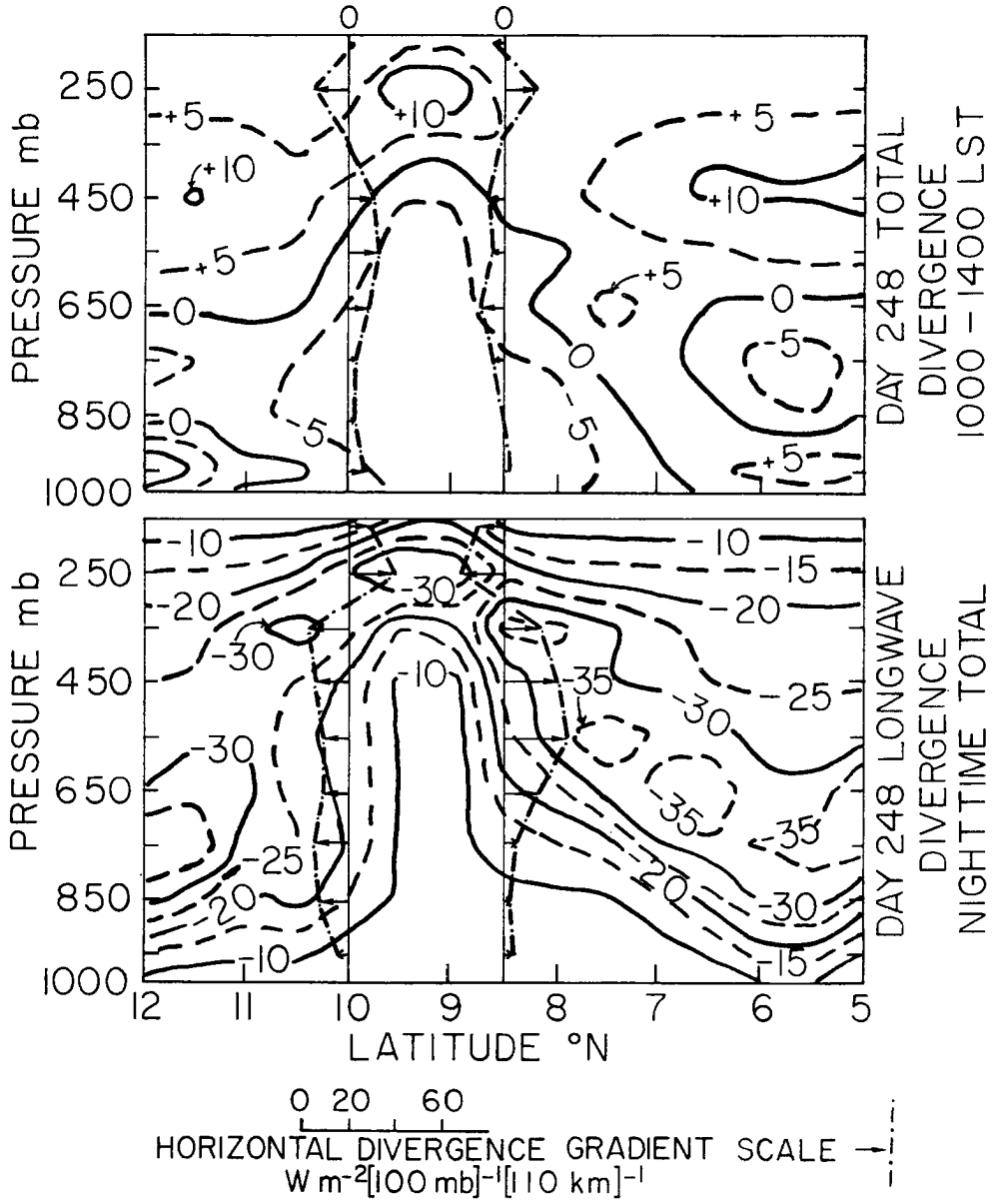

Fig. 19. A pressure vs. latitude (at 23.5°W longitude) cross-sectional view of the A/B-scale array for the 0600-1800 LST period of Day 248. The top portion of the figure depicts the 1000-1400 LST total (SW plus LW) radiative divergence (Wm^{-2}-100 mb^{-1}) and the bottom portion depicts the LW component only (nighttime total). Also shown is the magnitude and direction of the horizontal radiative divergence gradient at two points (arrows point towards regions of greater divergence). Cox and Griffith (1978).

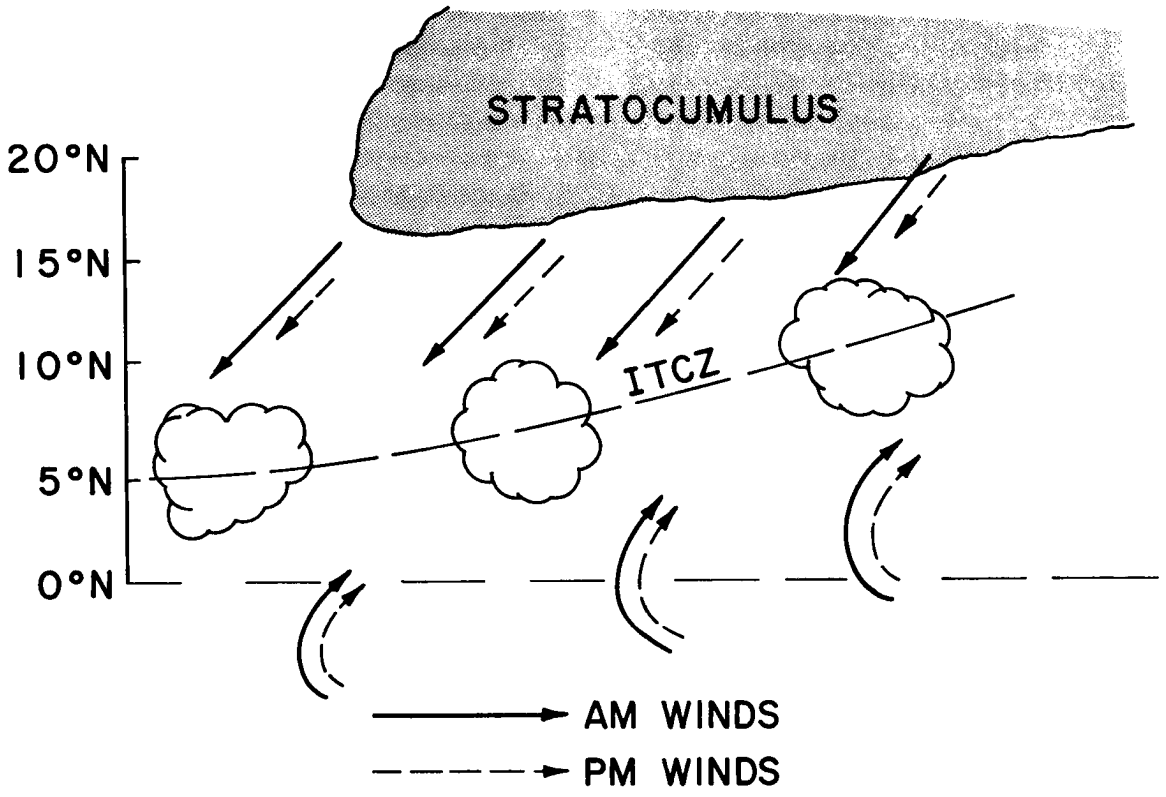

Fig. 20. Idealized model of diurnal oscillation of GATE region ITCZ. Solid streamlines represent morning circulation, broken streamlines represent evening circulation.

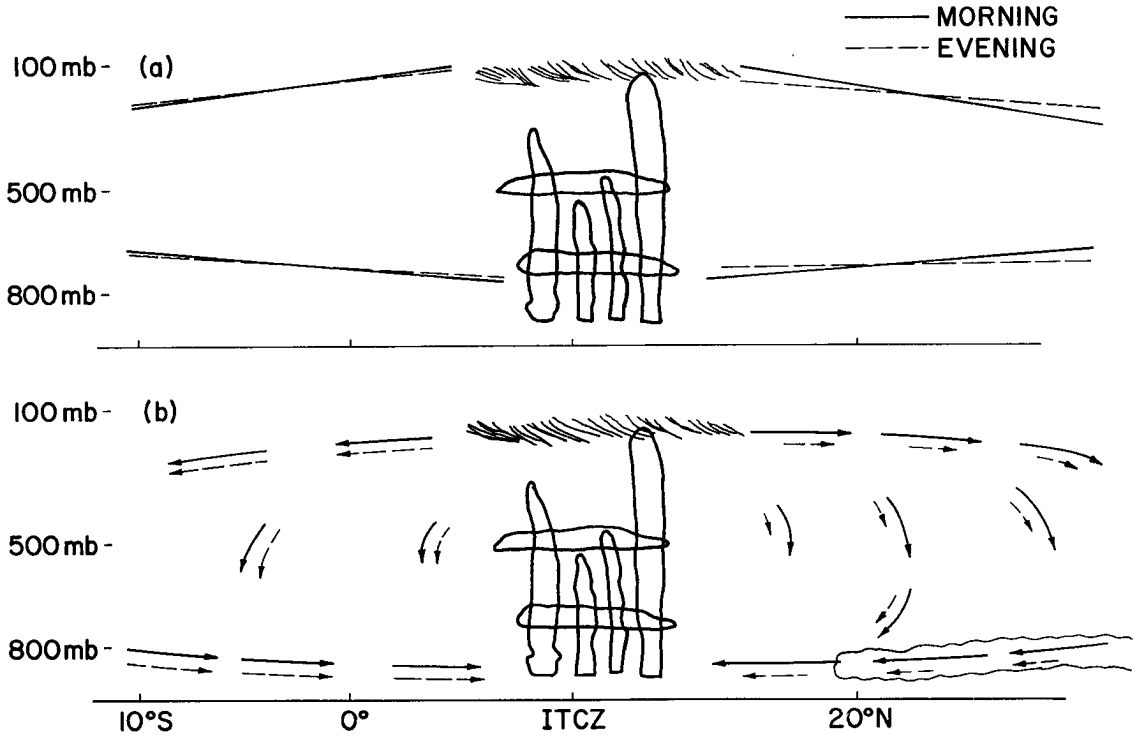

Fig. 21. Idealized model of the diurnal variation of the ITCZ mass circulation with the hypothesized slope of the pressure surfaces (a) and the resulting wind circulation (b). The solid line represents the typical morning circulation, the dashed curve the evening circulation.

A/B-scale during Phase III. Significant differences are found between the enhanced and suppressed case average Q_R's in the budget analysis with larger cooling diagnosed in the suppressed cases. Cox and Griffith do not show this difference in their Phase III data set which lacks strongly suppressed days.

The budgets of this paper diagnose large day-night radiational differences in each convective regime as does the Cox and Griffith Phase III data. It is gratifying that the budgets are able to diagnose physically realistic radiational differences between day and night and also between suppressed and enhanced conditions. This lends some confidence to the A/B-scale rawinsonde data and the budget method.

An attempt was also made to diagnose Q_R in the vertical by partitioning the net condensation minus evaporation level by level in the vertical with a simplified cloud model. The vertical profile of Q_R for the average of the all-GATE case and enhanced case appears reasonable. However, the condensation minus evaporation assumption does not appear to work very well in the suppressed cases and produces unrealistic looking Q_R profiles. Also, the smaller data sets at individual time periods were not able to diagnose physically consistent vertical distributions of Q_R at each time period. It is hoped that this beginning attempt at solving for radiation in the vertical as a residual will stimulate further research and refinement to this end. This work shows that it may be possible to use the budget analysis method as an alternative approach to determining the vertical distribution of radiational cooling.

Beyond all else, it is hoped that this study has shown, even to the skeptic's satisfaction, that a significant single cycle diurnal range in mass convergence is occurring in the GATE A/B-array and that this diurnal range is similar to that observed in the other oceans.

ACKNOWLEDGEMENTS

The author gratefully acknowledges Professor William M. Gray for his guidance and support of this research. I also thank Mr. Edwin Buzzell, Mr. Charles Solomon and Ms. Elizabeth Keim for their extensive computer programming assistance. Special thanks are due to Ms. Barbara Brumit and Ms. Dianne Schmitz for their assistance in manuscript preparation and data reduction. The author would also like to acknowledge the helpful discussions she has had on this subject with Dr. William M. Frank and Mr. John L. McBride. The effort of Dr. Stephen Cox in reviewing this paper is gratefully acknowledged.

This research has been supported by the National Science Foundation Grant No. ATM75-01424 A02.

BIBLIOGRAPHY

Albrecht, B. and S. K. Cox, 1975: The large-scale response of the tropical atmosphere to cloud-modulated infrared heating. J. Atmos. Sci., 32, 16-24.

Cox, S. K., 1969a: Radiation models of midlatitude synoptic features. Mon. Wea. Rev., 97, 637-651.

Cox, S. K., 1969b: Observational evidence of anomalous infrared cooling in the clear tropical atmosphere. J. Atmos. Sci., 26, 1347-1349.

Cox, S. K., 1971a: Infrared radiation models for the tropics. Proceedings of the Miami Workshop on Remote Sensing, NOAA, Boulder, CO, 161-178 [Available from NOAA ERL Labs., Boulder, CO].

Cox, S. K., 1971b: Cirrus clouds and the climate. J. Atmos. Sci., 28, 1513-1515.

Cox, S. K. and K. T. Griffith, 1978: Tropospheric radiative divergence during Phase III of the GARP Atlantic Tropical Experiment (GATE). Atmos. Sci. Paper No. 291, Colo. State Univ., Ft. Collins, CO, 166 pp.

Cunning, J. B. and R. I. Sax, 1977: A Z-R relationship for the GATE B-scale array. Mon. Wea. Rev., 105, 10, 1330-1336.

Fingerhut, W. A., 1978: A numerical model of a diurnally varying tropical cloud cluster disturbance. Mon. Wea. Rev., 106, 255-264.

Fleming, J. R. and S. K. Cox, 1974: Radiative effects of cirrus clouds. J. Atmos. Sci., 31, 2182-2188.

Foltz, G. S., 1976: Diurnal variation of the tropospheric energy budget. Atmos. Sci. Paper No. 262, Colo. State Univ., Ft. Collins, CO, 140 pp.

Frank, W. M., 1978: Diagnostic analysis of the GATE A/B-scale array at individual time periods. Atmos. Sci. Paper No. 297, Colo. State Univ., Ft. Collins, CO, 102 pp.

Gray, W. M., 1973: Cumulus convection and larger scale circulations, Part I: Broadscale and meso-scale interactions. Mon. Wea. Rev. 101, 839-855.

Gray, W. M., 1976: Diurnal variation of oceanic deep cumulus convection Paper II: Physical hypothesis. Atmos. Sci. Paper No. 243, Colo. State Univ., Ft. Collins, CO, 106 pp.

Gray, W. M. and R. W. Jacobson, Jr., 1977: Diurnal variation of deep cumulus convection. Mon. Wea. Rev., 105, 1171-1188.

BIBLIOGRAPHY (cont'd)

Gray, W. M., W. Frank, J. Dewart, P. Grube, J. McBride, E. Núñez, E. Buzzell, C. Solomon, D. Schmitz and B. Brumit, 1977: Analysis of GATE rawinsonde and precipitation data and comparison with other tropical regions and weather systems. Informal report, Dept. of Atmos. Sci., Colo. State Univ., Ft. Collins, CO.

Grube, P. G., 1978: Forthcoming M. S. Thesis on influence of deep cumulus convection on upper tropospheric temperature changes in GATE. Dept. of Atmos. Sci., Colo. State Univ., Ft. Collins, CO, 80523.

Henry, W. K., 1974: The tropical rainstorm. Mon. Wea. Rev., 102, 717-725.

Holle, R. L., S. Leavitt, J. Simpson, R. Biodini and J. Snow, 1977: Cloudiness from whole sky pictures taken aboard 4 U. S. B-scale ships. Dept. of Environmental Science Rept., Univ. of Virginia, Charlotteville, VA.

Hudlow, M. D., 1977: Diurnal variability of GATE precipitation from B-scale radar data. Rept. of the U. S. GATE Central Program Workshop, NOAA, Rockville, MD, 20852.

Jacobson, R. W. and W. M. Gray, 1976: Diurnal variation of oceanic deep cumulus convection. Dept. of Atmos. Sci. Paper No. 243, Colo. State Univ., Ft. Collins, CO, 106 pp.

McBride, J. L. and W. M. Gray, 1978: Mass divergence in tropical weather systems, Paper I: Diurnal variation, Paper II: Large-scale controls on convection. Dept. of Atmos. Sci. Paper No. 299, Colo. State Univ., Ft. Collins, CO.

McGarry, M. M. and R. J. Reed, 1978: Diurnal variations in convective activity and precipitation during Phases II and III of GATE. Mon. Wea. Rev., 106, 101-113.

Nitta, T., 1977: Response of cumulus updraft and downdraft to GATE A/B-scale motion systems. J. Atmos. Sci., 34, 1163-1186.

Ooyama, V. and S. Esbensen, 1978: Rawinsonde data quality. Rept. of the U. S. GATE Central Program Workshop. NOAA, Rockville, MD, 20852, 131-161.

Reed, R. J., D. C. Norquist and E. E. Recker, 1977: The structure and properties of African wave disturbances as observed during Phase III of GATE. Mon. Wea. Rev., 105, 317-333.

Reeves, R., S. Williams, E. Rasmussen, D. Acheson, T. Carpenter and J. Rasmussen, 1976: GATE convection subprogram data center-analysis of rawinsonde intercomparison data. NOAA Tech. Rept, EDSZO, 75 pp.

BIBLIOGRAPHY (cont'd)

Ruprecht, E. and W. M. Gray, 1976: Analysis of satellite observed tropical cloud clusters, Paper II: Thermal, moisture and precipitation. Tellus, 28, 414-426.

Seguin, W. R. and P. Sabol, 1976: Shipboard precipitation data. NOAA Technical Rept. EDS 18, 62 pp.

Yanai, M., S. Esbensen and J. H. Chu, 1973: Determination of bulk properties of tropical cloud clusters from large-scale heat and moisture budgets. J. Atmos. Sci., 30, 611-627.

APPENDIX A

Various data quality summaries have been presented (Reeves et al., 1976; Ooyama and Esbensen, 1978; Gray et al., 1977) concerning the reliability of the GATE A/B and B-scale upper air and thermodynamic data. Reeves et al. (1976) and Ooyama and Esbensen (1978) have all commented upon the high frequency noise in the wind data from U.S. radiosondes tracked with the OMEGA/VLF systems. This fact, combined with the greater frequency of missing rawinsonde reports from the B-scale ships than from the A/B-scale ships during Phase I and II, determined that only A/B-scale winds would be used in this study. The accuracy of the winds is attested by the small mass balance corrections necessary to add to each wind report to force the vertical motions to zero at 100 mb. These mass balanced corrections are listed in Table A1 for each case.

Ooyama and Esbensen also noted that the solar radiation correction applied to the USSR (A/B-scale) temperatures produced temperature maxima near midnight and minima near noon. So, for the heat and moisture budgets the storage term was replaced with B-scale data. For ease of computation, however, A/B-scale winds and thermodynamic data were used in the horizontal and vertical convergence terms of the budgets. As the convergence terms are primarily influenced by the wind divergence changes rather than T or q changes, the convergence terms are still quite accurate.

The individual time period budgets for the suppressed case required some modification of the wind and specific humidity data. Using A/B winds and B-array temperatures and humidities, the moisture budget

TABLE 18

Divergence Mass Balance Corrections

$$V_R \text{ (corrected)} = V_R \text{ (observed)} - \Delta V_R$$

Data Set		A/B ΔV_R (m/sec)
ALL GATE AVERAGE		.01
ENHANCED AVERAGE		.04
SUPPRESSED AVERAGE		-.07
ALL GATE	00Z	-.01
	06Z	.03
	12Z	.11
	18Z	-.08
ENHANCED	00Z	-.01
	06Z	.15
	12Z	.15
	18Z	-.08
SUPPRESSED	00Z	.03
	06Z	-.15
	12Z	.12
	18Z	-.27

at 18Z yielded negative P_o and an unrealistic Q_R value of -3.7^oC/day at 06Z. The cause for these problems is uncertain. To compute the moisture and energy budgets A/B-scale q's were averaged with the B-scale data for the storage term in the individual time period suppressed case moisture budgets. Upper level sinking at 18Z was also reduced by 25% between 450 mb and 200 mb to reduce the large mean sinking drying in the suppressed case. These modifications allowed a positive P_o to be calculated at 18Z.

The large Q_R calculated at 06Z in the suppressed case was reduced by lowering the sinking motion at 250 mb to 450 mb by $\sim$ 15%. This large sinking and convergence of static energy aloft required a large Q_R to balance the heat budget as the observed temperature changes were not large enough to be consistent with the import of static energy.

APPENDIX B

The level by level moisture and heat budgets by diurnal time periods for the all GATE, enhanced and suppressed cases are presented in Tables 19 to 30.

TABLE 19

ALL GATE 00Z

PRESSURE (10^2mb)	mb/d $\bar{\omega}$	gm/cm^{2}d $\overline{\nabla \cdot Vq}$	gm/cm^{2}d $\frac{\bar{\omega}\,\bar{q}}{g}$	gm/cm^{2}d $\frac{\partial q}{\partial t}$	gm/cm^{2}d (c-e)	gm/cm^{2}d $\frac{\overline{\omega' q'}}{g}$	gm/cm^{2}d $\frac{\partial}{\partial p}\frac{(\overline{\omega' q'})}{g}$	gm/cm^{2}d Total (c-e)	°C/d Total (c-e)	°C/d $Q_1 - S_o$	°C/d Q_R	°C/d Smoothed Q_R
-1												
-	11		0									
-2		0		0	0			0	0	-2.2	-2.2	-2.2
-	-3		0									
-3		0		0	.03			.03	.7	-1.0	-1.7	-1.7
-	-19		.03↑									
-4		-.02		-.01	.03			.03	.7	-.4	-1.1	-1.4
-	-8		.03↑									
-5		.01		-.02	.07		.01	.08	1.4	.1	-1.8	-1.4
-	-14		.09↑			.01↑						
-6		.04		-.02	.13		.04	.17	4.1	1.0	-3.1	-3.1
-	-26		.24↑			.05↑						
-7		.07		-.02	.17		.08	.25	1.0	1.4	-4.6	-4.3
-	-38		.46↑			.13↑						
-8		+.12		0	.19		.11	.30	7.2	2.4	-4.8	-4.4
-	-54		.77↑			.24↑						
-9		-.30		.01	.11		.12	.23	5.5	2.1	-3.4	-3.4
-	-34		.59↑			.36↑						
-10		-.51		.01						-2.0	-2.0	-2.0
			E_o = .45									
TOTAL		-0.59		-.05	.73		.36	1.09				-2.7

TABLE 20

ALL GATE 06Z

PRESSURE (10^2mb)	$\overline{\omega}$ mb/d	$\overline{\nabla \cdot Vq}$ gm/cm^{2}d	$\frac{\overline{\omega}\,\overline{q}}{g}$ gm/cm^{2}d	$\frac{\partial q}{\partial t}$ gm/cm^{2}d	(c-e) gm/cm^{2}d	$\frac{\overline{\omega' q'}}{g}$ gm/cm^{2}d	$\frac{\partial}{\partial p}\frac{(\overline{\omega' q'})}{g}$ gm/cm^{2}d	Total (c-e) gm/cm^{2}d	Total (c-e) °C/d	$Q_1 - S_o$ °C/d	Q_R °C/d	Smoothed Q_R °C/d
-1												
	6		0									
-2		0		0	0		0	0	0	0	0	0
	-1		0									
-3		0		-.01	.06	.01↑	.01	.07	1.7	1.5	-.2	-.3
	-28		.05↑									
-4		0		-.03	.12	.02↑	.01	.13	3.1	2.4	-0.7	-1.0
	-35		.14↑									
-5		.03		-.03	.21	.05↑	.03	.24	5.8	3.4	-2.4	-2.2
	-54		.35↑									
-6		.04		-.03	.21	.12↑	.07	.28	6.7	3.5	-3.2	-3.6
	-62		.57↑									
-7		.02		-.03	.28	.22↑	.10	.38	9.1	3.5	-5.6	-4.9
	-70		.84↑									
-8		.02		-.02	.17	.34↑	.12	.29	7.0	4.1	-2.9	-3.9
	-71		1.01↑									
-9		-.47		-.04	.19	.45↑	.11	.30	7.2	2.9	-4.3	-3.2
	-40		.69↑									
-10		-.65		-.02						-1.2	-1.2	-1.2
			E_o= .47↑									
TOTAL		-1.01		-.21	1.24		.45	1.69				-2.3

TABLE 21

ALL GATE 12Z

PRESSURE (10^2mb)	mb/d $\bar{\omega}$	gm/cm^{2}d $\overline{\nabla \cdot Vq}$	gm/cm^{2}d $\frac{\bar{\omega}\,\bar{q}}{g}$	gm/cm^{2}d $\frac{\partial q}{\partial t}$	gm/cm^{2}d (c-e)	gm/cm^{2}d $\frac{\overline{\omega' q'}}{g}$	gm/cm^{2}d $\frac{\partial}{\partial p}\frac{(\overline{\omega' q'})}{g}$	gm/cm^{2}d Total (c-e)	^{o}C/d Total (c-e)	^{o}C/d $Q_1 - S_o$	^{o}C/d Q_R	^{o}C/d Smoothed Q_R
-1												
	+1		0									
-2		0		0	.01		.01	.02	.4	.9	.5	.5
	-27		.01↑			.01↑						
-3		0		0	.08		.01	.09	2.2	3.0	.8	.0
	-51		.09↑			.02↑						
-4		0		.01	.16		.02	.18	4.3	4.5	.2	.1
	-63		.26↑			.04↑						
-5		.03		.02	.25		.03	.28	6.7	5.9	-.8	-1.0
	-87		.56↑			.07↑						
-6		.03		.02	.30		.05	.35	8.4	6.0	-2.4	-2.4
	-99		.91↑			.12↑						
-7		-.01		.02	.31		.09	.40	9.6	5.4	-4.2	-3.2
	-102		1.23↑			.21↑						
-8		-.09		0	.24		.10	.34	8.2	6.0	-2.2	-2.2
	-97		1.38↑			.31↑						
-9		-.63		-.01	.08		.09	.17	4.1	3.9	-.2	-.8
	-47		.82↑			.40↑						
-10		-.74		-.01						-.8	-.8	-.8
			E_o=.47↑									
TOTAL		-1.41		.05	1.43		.40	1.83				-1.0

TABLE 22

ALL GATE 18Z

PRESSURE (10^2mb)	mb/d $\overline{\omega}$	gm/cm^{2}d $\overline{\nabla \cdot Vq}$	gm/cm^{2}d $\frac{\overline{\omega}\ \overline{q}}{g}$	gm/cm^{2}d $\frac{\partial q}{\partial t}$	gm/cm^{2}d (c-e)	gm/cm^{2}d $\frac{\overline{\omega' q'}}{g}$	gm/cm^{2}d $\frac{\partial}{\partial p}\frac{(\overline{\omega' q'})}{g}$	gm/cm^{2}d Total (c-e)	^{o}C/d Total (c-e)	^{o}C/d $Q_1 - S_o$	^{o}C/d Q_R	^{o}C/d Smoothed Q_R
-1												
	-6		0									
-2		0		0	.02			.02	.4	-1.0	-1.4	-1.4
	-45		.02↑									
-3		0		.01	.09	.01↑	.01	.10	2.4	1.3	-1.1	-1.0
	-63		.12↑									
-4		-.02		.03	.11	.02↑	.01	.12	2.9	2.7	-.2	-.6
	-60		.24↑									
-5		0		.03	.17	.06↑	.04	.21	5.0	3.9	-1.1	-1.2
	-69		.44↑									
-6		.01		.03	.23	.11↑	.05	.28	6.7	4.1	-2.6	-2.4
	-77		.71↑									
-7		.02		.03	.23	.18↑	.07	.30	7.2	3.8	-3.4	-2.8
	-82		.99↑									
-8		-.03		.02	.18	.28↑	.10	.28	6.7	4.8	-1.9	-1.8
	-82		1.16↑									
-9		-.51		.04	.06	.36↑	.08	.14	3.4	3.2	-.2	-1.0
	-43		.75↑									
-10		-.66		.02						-1.8	-1.8	-1.8
			E_o = .47↑									
TOTAL		-1.19		.21	1.09		.36	1.45				-1.5

TABLE 23

A/B ENHANCED OOZ

PRESSURE (10^2mb)	mb/d $\overline{\omega}$	gm/cm^{2}d $\overline{\nabla \cdot Vq}$	gm/cm^{2}d $\frac{\overline{\omega}\,\overline{q}}{g}$	gm/cm^{2}d $\frac{\partial q}{\partial t}$	gm/cm^{2}d (c-e)	gm/cm^{2}d $\frac{\overline{\omega' q'}}{g}$	gm/cm^{2}d $\frac{\partial}{\partial p}\frac{(\overline{\omega' q'})}{g}$	gm/cm^{2}d Total (c-e)	^{o}C/d Total (c-e)	^{o}C/d $Q_1 - S_o$	^{o}C/d Q_R	^{o}C/d Smoothed Q_R
-1												
	13		0									
-2		0		0	0			0	0	-2.0	-2.0	-2.0
	-7		0									
-3		0		.02	.05			.05	1.2	-.1	-1.3	-1.4
	-41		.07↑									
-4		-.02		.04	0	.01↑	.01	.01	.2	1.1	.9	-.3
	-23		.09↑									
-5		.04		.01	.11	.02↑	.01	.12	2.9	1.4	-1.5	-1.7
	-39		.25↑									
-6		.15		0	.29	.05↑	.03	.32	7.7	3.1	-4.6	-4.0
	-75		.69↑									
-7		.20		.07	.33	.11↑	.06	.39	9.4	4.0	-5.4	-5.1
	-107		1.29↑									
-8		.01		.08	.35	.21↑	.10	.45	10.8	5.5	-5.3	-4.2
	-121		1.73↑									
-9		-.77		.03	.06	.33↑	.12	.18	4.3	3.2	-1.1	-2.5
	-60		1.05↑									
-10		-.93		0						-2.5	-2.5	-2.5
			E_o = .45↑									
TOTAL		-1.32		.25	1.19		.33	1.52				-2.6

TABLE 24

A/B ENHANCED 06Z

PRESSURE (10^2mb)	mb/d $\bar{\omega}$	gm/cm^{2}d $\overline{\nabla \cdot Vq}$	gm/cm^{2}d $\frac{\bar{\omega}\,\bar{q}}{g}$	gm/cm^{2}d $\frac{\partial q}{\partial t}$	gm/cm^{2}d (c-e)	gm/cm^{2}d $\frac{\overline{\omega' q'}}{g}$	gm/cm^{2}d $\frac{\partial}{\partial p}\frac{(\overline{\omega' q'})}{g}$	gm/cm^{2}d Total (c-e)	^{o}C/d Total (c-e)	^{o}C/d $Q_1 - S_o$	^{o}C/d Q_R	^{o}C/d Smoothed Q_R
-1												
	11											
-2		.01		0	0			0	0	.2	.2	.2
	-21		.01↑									
-3		.01		-.01	.05		.01	.06	1.4	2.0	.6	.2
	-33		.06↑			.01↑						
-4		0		-.01	.12		.02	.14	3.4	2.9	-.5	-.2
	-42		.17↑			.03↑						
-5		.10		.04	.21		.01	.22	5.3	5.0	-.3	-1.5
	-81		.52↑			.04↑						
-6		.23		.07	.43		.03	.46	11.0	6.2	-4.8	-3.8
	-136		1.25↑			.07↑						
-7		.17		.08	.47		.05	.52	12.5	7.2	-5.3	-3.9
	-163		1.97↑			.12↑						
-8		-.10		.05	.29		.07	.36	8.6	8.6	0	-2.6
	-155		2.21↑			.19↑						
-9		-1.04		-.04	.33		.06	.39	9.4	4.5	-4.9	-3.1
	-84		1.46↑			.25↑						
-10		-1.22		.02						-2.6	-2.6	-2.6
			E_o = .51↑									
TOTAL		-1.84		.20	1.90		.25	2.15				-1.9

TABLE 25

A/B ENHANCED 12Z

PRESSURE (10^2mb)	$\overline{\omega}$ mb/d	$\overline{\nabla \cdot Vq}$ gm/cm^{2}d	$\frac{\overline{\omega}\,\overline{q}}{g}$ gm/cm^{2}d	$\frac{\partial q}{\partial t}$ gm/cm^{2}d	(c-e) gm/cm^{2}d	$\frac{\overline{\omega' q'}}{g}$ gm/cm^{2}d	$\frac{\partial}{\partial p}\left(\frac{\overline{\omega' q'}}{g}\right)$ gm/cm^{2}d	Total (c-e) gm/cm^{2}d	Total (c-e) °C/d	$Q_1 - S_o$ °C/d	Q_R °C/d	Smoothed Q_R °C/d
-1													
-	-10		0										
-2		.01		0	.01		.01	.02	.4	2.8	2.4	2.4	
-	-40		.02↑			.01↑							
-3		.01		.01	.14		.02	.16	3.6	6.0	2.4	2.4	
-	-99		.18↑			.02↑							
-4		.03		.08	.22		.02	.24	5.8	8.3	2.5	2.5	
-	-126		.51↑			.04↑							
-5		.13		.19	.31		.03	.34	8.2	11.0	2.8	1.9	
-	-177		1.14↑			.07↑							
-6		.14		.21	.49		.06	.55	13.2	12.7	-.5	-.3	
-	-215		1.98↑			.13↑							
-7		-.05		.15	.49		.08	.57	13.7	10.8	-2.9	-1.5	
-	-214		2.57↑			.21↑							
-8		-.35		.05	.35		.10	.45	10.8	11.1	.3	-.3	
-	-183		2.62↑			.31↑							
-9		-1.26		-.05	.11		.08	.19	4.6	5.7	1.1	.1	
-	-81		1.42↑			.39↑							
-10		-1.27		-.04						-2.0	-2.0	-2.0	
			E_o = .50↑										
TOTAL		-2.61		.60	2.12		.39	2.51					.7

TABLE 26

A/B ENHANCED 18Z

PRESSURE (10^2mb)	mb/d $\overline{\omega}$	gm/cm^{2}d $\overline{\nabla \cdot Vq}$	gm/cm^{2}d $\frac{\overline{\omega}\,\overline{q}}{g}$	gm/cm^{2}d $\frac{\partial q}{\partial t}$	gm/cm^{2}d (c-e)	gm/cm^{2}d $\frac{\overline{\omega' q'}}{g}$	gm/cm^{2}d $\frac{\partial}{\partial p}\frac{(\overline{\omega' q'})}{g}$	gm/cm^{2}d Total (c-e)	°C/d Total (c-e)	°C/d $Q_1 - S_o$	°C/d Q_R	°C/d Smoothed Q_R
-1												
-	-12		0									
-2		.01		0	.03			.03	.7	.9	.2	.2
-	-87		.04↑									
-3		0		.02	.18			.18	4.3	4.4	.1	.4
-	-133		.24↑									
-4		.01		.07	.27			.27	6.5	7.6	1.1	.8
-	-145		.59↑									
-5		.04		.09	.36	.01↑	.01	.37	8.9	9.9	1.0	-.1
-	-167		1.08↑									
-6		.03		.08	.53	.06↑	.05	.58	13.9	10.4	-3.5	-2.6
-	-187		1.72↑									
-7		-.01		.03	.54	.14↑	.08	.62	14.4	9.8	-4.6	-3.8
-	-190		2.28↑									
-8		-.29		-.04	.49	.23↑	.09	.58	13.9	11.1	-2.8	-1.5
-	-171		2.44↑									
-9		-1.04		-.04	-.07	.37↑	.14	.07	1.7	5.8	-4.1	.8
-	-74		1.29↑									
-10		-1.11		-.01						-2.0	-2.0	-2.0
			E_o = .54↑									
TOTAL		-2.36		.20	2.33		.37	2.70				-.8

TABLE 27

A/B SUPPRESSED 00Z

PRESSURE (10^2mb)	mb/d $\bar{\omega}$	gm/cm^{2}d $\overline{\nabla \cdot \nabla q}$	gm/cm^{2}d $\frac{\bar{\omega}\,\bar{q}}{g}$	gm/cm^{2}d $\frac{\partial q}{\partial t}$	gm/cm^{2}d (c-e)	gm/cm^{2}d $\frac{\overline{\omega' q'}}{g}$	gm/cm^{2}d $\frac{\partial}{\partial p}\frac{(\overline{\omega' q'})}{g}$	gm/cm^{2}d Total (c-e)	°C/d Total (c-e)	°C/d $Q_1 - S_o$	°C/d Q_R	°C/d Smoothed Q_R
-1												
	8		0									
-2		0		0	0		0	0	0	-2.5	-2.5	-2.5
	10		0									
-3		0	.01↓	-.01	0	.01↑	.01	.01	.2	-1.9	-2.1	-2.4
	14											
-4		0	.06↓	-.02	-.03	.06↑	.05	.02	.5	-2.4	-2.9	-2.4
	27											
-5		.03	.04↓	-.01	0	.07↑	.01	.01	.2	-1.6	-1.8	-1.8
	11											
-6		.03	.01↓	-.04	.04	.08↑	.01	.05	1.2	.5	-.7	-1.3
	1											
-7		.03	.09↑	-.04	.11	.09↑	.01	.12	2.9	.9	-2.0	-1.4
	-8											
-8		.17	.28↑	-.02	.04	.16↑	.07	.11	2.6	1.5	-1.1	-1.9
	-19											
-9		-.08	.36↑	.02	.14	.25↑	.09	.23	5.5	1.9	-3.6	-2.4
	-21											
-10		-.24		.01						-1.2	-1.2	-1.2
			E_o = .38↑									
TOTAL		-.06		-.11	.30		.25	.55				-1.9

TABLE 28

A/B SUPPRESSED 06Z

PRESSURE (10^2mb)	mb/d $\overline{\omega}$	gm/cm^{2}d $\overline{\nabla \cdot Vq}$	gm/cm^{2}d $\frac{\overline{\omega}\,\overline{q}}{g}$	gm/cm^{2}d $\frac{\partial q}{\partial t}$	gm/cm^{2}d (c-e)	gm/cm^{2}d $\frac{\overline{\omega' q'}}{g}$	gm/cm^{2}d $\frac{\partial}{\partial p}\left(\frac{\overline{\omega' q'}}{g}\right)$	gm/cm^{2}d Total (c-e)	^{o}C/d Total (c-e)	^{o}C/d $Q_1 - S_o$	^{o}C/d Q_R	^{o}C/d Smoothed Q_R
-1												
-	17		0									
-2		0		0	-.01	.01↑	.01	0	0	.7	.7	.7
-	30		.01↓									
-3		-.01		-.03	.01	.03↑	.02	.03	.7	-.9	-1.6	-1.4
-	42		.04↓									
-4		-.01		-.07	.01	.08↑	.05	.06	1.4	-1.7	-3.1	-3.2
-	51		.11↓									
-5		.03		-.09	.01	.18↑	.10	.11	2.6	-2.5	-5.1	-4.5
-	40		.16↓									
-6		.08		-.10	0	.30↑	.12	.12	2.9	-1.8	-4.7	-5.0
-	30		.18↓									
-7		.08		-.12	.07	.42↑	.12	.19	4.6	-.7	-5.3	-4.2
-	19		.15↓									
-8		.29		-.14	0	.48↑	.06	.06	1.4	-.3	-1.7	-3.2
-	0		0									
-9		-.01		.05	.16	.55↑	.07	.23	5.5	9	-4.6	-2.7
-	-12		.20↓									
-10		-.37		-.03						-.1	-.1	-.1
			$E_o = .35\uparrow$									
TOTAL		.08		-.53	.26		.54	.80				-2.7

TABLE 29

A/B SUPPRESSED 12Z

PRESSURE (10^2mb)	mb/d $\overline{\omega}$	gm/cm^{2}d $\overline{\nabla \cdot Vq}$	gm/cm^{2}d $\frac{\overline{\omega}\,\overline{q}}{g}$	gm/cm^{2}d $\frac{\partial q}{\partial t}$	gm/cm^{2}d (c-e)	gm/cm^{2}d $\frac{\overline{\omega' q'}}{g}$	gm/cm^{2}d $\frac{\partial}{\partial p}\frac{(\overline{\omega' q'})}{g}$	gm/cm^{2}d Total (c-e)	°C/d Total (c-e)	°C/d $Q_1 - S_o$	°C/d Q_R	°C/d Smoothed Q_R
-1												
-2	2	0	0	0	0			0	0	-1.2	-1.2	-1.2
-3	21	0	0	-.01	0		.01	.01	.2	-.1	-.3	-.6
-4	9	0	.01↓	-.01	.03	.01↑	.03	.06	1.4	.8	-.6	-.7
-5	-3	.01	.01↑	-.01	.10	.04↑	.02	.12	2.9	1.5	-1.4	-.8
-6	-17	.01	.11↑	-.01	.02	.06↑	.03	.05	1.2	1.4	.2	-.4
-7	-15	.03	.13↑	.01	.04	.09↑	.05	.09	2.2	1.6	-.6	-.6
-8	-17	.19	.21↑	.02	.04	.14↑	.10	.14	3.4	2.0	-1.4	-1.8
-9	-33	-.18	.46↑	.01	.14	.24↑	.12	.26	6.2	2.4	-3.8	-2.1
-10	-25	-.43	.43↑	.01		.36↑				.4	.4	.4
			E_o=.37↑									
TOTAL		-.37		.01	.37		.36	.73				-.9

TABLE 30

A/B SUPPRESSED 18Z

PRESSURE (10^2mb)	mb/d $\overline{\omega}$	gm/cm^{2}d $\overline{\nabla \cdot Vq}$	gm/cm^{2}d $\frac{\overline{\omega}\,\overline{q}}{g}$	gm/cm^{2}d $\frac{\partial q}{\partial t}$	gm/cm^{2}d (c-e)	gm/cm^{2}d $\frac{\overline{\omega' q'}}{g}$	gm/cm^{2}d $\frac{\partial}{\partial p}\frac{(\overline{\omega' q'})}{g}$	gm/cm^{2}d Total (c-e)	°C/d Total (c-e)	°C/d $Q_1 - S_o$	°C/d Q_R	°C/d Smoothed Q_R
-1												
	2		0			0						
-2		0		0	-.01		.01	0	0	-2.7	-2.7	-2.4
	36		.01↓			.01↑						
-3		0		0	-.03		.03	0	0	-2.5	-2.5	-2.7
	38		.04↓			.04↑						
-4		0		-.01	-.03		.03	0	0	-3.1	-3.1	-2.8
	36		.08↓			.07↑						
-5		.04		-.05	0		.02	.02	.5	-2.2	-2.7	-2.7
	22		.09↓			.09↑						
-6		.04		-.07	.04		.02	.06	1.4	-1.0	-2.4	-2.0
	13		.08↓			.11↑						
-7		.02		0	-.02		.03	.01	.2	-.3	-.5	-.9
	10		.08↓			.14↑						
-8		.13		.07	-.08		.09	.01	.2	.1	-.1	-.2
	-3		.04↑			.23↑						
-9		.11		.11	-.06		.08	.02	.5	.4	-.1	-.6
	-11.2		.20↑			.31↑						
-10		-.18		.03						-2.0	-2.0	-2.0
			E_o=.36↑									
TOTAL		.16		.08	-.19		.31	.12				-1.8

W. M. GRAY'S FEDERALLY SUPPORTED RESEARCH PROJECT REPORTS SINCE 1967

CSU Dept. of Atmos. Sci. Report No.	Report Title, Author, Date, Agency Support
104	The Mutual Variation of Wind, Shear, and Baroclinicity in the Cumulus Convective Atmosphere of the Hurricane (69pp). W. M. Gray. February 1967. NSF Support.
114	Global View of the Origin of Tropical Disturbances and Storms (105pp). W. M. Gray. October 1967. NSF Support.
116	A Statistical Study of the Frictional Wind Veering in the Planetary Boundary Layer (57pp). B. Mendenhall. December 1967. NSF and ESSA Support.
124	Investigation of the Importance of Cumulus Convection and Ventilation in Early Tropical Storm Development (88pp). R. Lopez. June 1968. ESSA Satellite Lab. Support.
Unnumbered	Role of Angular Momentum Transports in Tropical Storm Dissipation over Tropical Oceans (46pp). R. F. Wachtmann. December 1968. NSF and ESSA Support.
Unnumbered	Monthly Climatological Wind Fields Associated with Tropical Storm Genesis in the West Indies (34pp). J. W. Sartor. December 1968. NSF Support.
140	Characteristics of the Tornado Environment as Deduced from Proximity Soundings (55pp). T. G. Wills. June 1969. NOAA and NSF Support.
161	Statistical Analysis of Trade Wind Cloud Clusters of the Western North Pacific (80pp). K. Williams. June 1970. ESSA Satellite Lab. Support.
---	A Climatology of Tropical Cyclones and Disturbances of the Western Pacific with a Suggested Theory for Their Genesis/ Maintenance. W. M. Gray. NAVWEARSCHFAC Technical Paper No. 19-70 (225pp). November 1970. (Available from U.S. Navy, Monterey, CA). U.S. Navy Support.
179	A Diagnostic Study of the Planetary Boundary Layer over the Oceans (95pp). W. M. Gray. February 1972. Navy and NSF Support.
182	The Structure and Dynamics of the Hurricane's Inner Core Area (105pp). D. J. Shea. April 1972. NOAA and NSF Support.
188	Cumulus Convection and Larger-Scale Circulation, Part I: A Parametric Model of Cumulus Convection (100pp). R. E. Lopez. June 1972. NSF Support.

CSU Dept. of Atmos. Sci. Report No.	Report Title, Author, Date, Agency Support
189	Cumulus Convection and Larger-Scale Circulations, Part II: Cumulus and Meso-Scale Interactions (63pp). R. E. Lopez. June 1972. NSF Support.
190	Cumulus Convection and Larger-Scale Circulations, Part III: Broadscale and Meso-Scale Considerations (80pp). W. M. Gray. July 1972. NOAA-NESS.
195	Characteristics of Carbon Black Dust as a Tropospheric Heat Source for Weather Modification (55pp). W. M. Frank. January 1973. NSF Support.
196	Feasibility of Beneficial Hurricane Modification by Carbon Black Seeding (130pp). W. M. Gray. April 1973. NOAA Support.
199	Variability of Planetary Boundary Layer Winds (157pp). L. R. Hoxit. May 1973. NSF Support.
200	Hurricane Spawned Tornadoes (57pp). D. J. Novlan. May 1973. NOAA and NSF Support.
212	A Study of Tornado Proximity Data and an Observationally Derived Model of Tornado Genesis (101pp). R. Maddox. November 1973. NOAA Support.
219	Analysis of Satellite Observed Tropical Cloud Clusters (91 pp). E. Ruprecht and W. M. Gray. May 1974. NOAA-NESS Support.
224	Precipitation Characteristics in the Northeast Brazil Dry Region (56pp). R. P. L. Ramos. May 1974. NSF Support.
225	Weather Modification through Carbon Dust Absorption of Solar Energy (190pp). W. M. Gray, W. M. Frank, M. L. Corrin, and C. A. Stokes. July 1974.
234	Tropical Cyclone Genesis (121pp). W. M. Gray. March 1975. NSF Support.
---	Tropical Cyclone Genesis in the Western North Pacific (66pp). W. M. Gray. March 1975. U.S. Navy Environmental Prediction Research Facility Report. Technical Paper No. 16-75. (Available from the U.S. Navy, Monterey, CA). Navy Support.
241	Tropical cyclone Motion and Surrounding Parameter Relationships (105pp). J. E. George. December 1975. NOAA Support.

CSU Dept. of Atmos. Sci. Report No.	Report Title, Author, Date, Agency Support
243	Diurnal Variation of Oceanic Deep Cumulus Convection. Paper I: Observational Evidence, Paper II: Physical Hypothesis (106pp). R. W. Jacobson, Jr. and W. M. Gray. February, 1976. NOAA NESS Support.
257	Data Summary of NOAA's Hurricane Inner-Core Radial Leg Flight Penetrations 1957-1967, and 1969 (245pp). W. M. Gray and D. J. Shea. October, 1976. NSF and NOAA Support.
258	The Structure and Energetics of the Tropical Cyclone (180 pp). W. M. Frank. October, 1976. NOAA (NHEML), NOAA (NESS) and NSF Support.
259	Typhoon Genesis and Pre-typhoon Cloud Clusters (79pp). R. M. Zehr. November, 1976.
Unnumbered	Severe Thunderstorm Wind Gusts (81pp). G. W. Walters. December, 1976. NSF Support.
262	Diurnal Variation of the Tropospheric Energy Budget (141 pp). G. S. Foltz. November, 1976. NSF Support.
274	Comparison of Developing vs Non-Developing Tropical Disturbances (81 pp). Steven L. Erickson. July, 1977. U.S. Army Support.
277	Tropical Cyclone Cloud and Intensity Relationships (154 pp). Charles P. Arnold. November, 1977. U.S. Army and NHEML Support.
297	Diagnostic Analyses of the GATE A/B-scale Area at Individual Time Periods (102 pp). W. M. Frank. November, 1978. NSF Support.
298	Diurnal Variability in the GATE Region (80 pp). Jean M. Dewart. November, 1978. NSF Support.
299	Mass Divergence in Tropical Weather Systems, Paper I: Diurnal Variation; Paper II: Large-scale Controls on Convection (109 pp). John. L. McBride and W. M. Gray. November, 1978. NOAA-NHEML Support.

BIBLIOGRAPHIC DATA SHEET	1. Report No. CSU-ATS-298	2.	3. Recipient's Accession No.
4. Title and Subtitle Diurnal Variability In The GATE Region			5. Report Date November, 1978 6.
7. Author(s) Jean M. Dewart			8. Performing Organization Rept. No. CSU-ATS-298
9. Performing Organization Name and Address Atmospheric Science Department Colorado State University Ft. Collins, CO 80523			10. Project/Task/Work Unit No. 11. Contract/Grant No. ATM75-01424 A02
12. Sponsoring Organization Name and Address National Science Foundation 18th and G. Streets, N.W. Washington, DC 20550			13. Type of Report & Period Covered Project report 14.

15. Supplementary Notes

16. Abstracts

This paper discusses the observational evidence for and the probable causes of the large diurnal variability of the atmosphere over the Inter Tropical Convergence Zone (ITCZ) region of the tropical eastern Atlantic Ocean. The analysis is based on the observational information of the A/B-scale rawinsonde data of the GARP Atlantic Tropical Experiment(GATE).

A large single cycle diurnal oscillation of wind divergence similar to that observed in the western Atlantic and western Pacific oceans is found. Maximum divergences occur in the late morning, minimum in the early evening. Boundary layer divergence profiles show almost identical divergence for both convectively enhanced and convectively suppressed conditions. Tropospheric diurnal temperature variation is also investigated.

17. Key Words and Document Analysis. 17a. Descriptors

GATE studies
Diurnal variation of tropical atmosphere
Tropospheric radiation
Tropical convection

17b. Identifiers/Open-Ended Terms

17c. COSATI Field/Group

18. Availability Statement	19. Security Class (This Report) UNCLASSIFIED	21. No. of Pages 80
	20. Security Class (This Page) UNCLASSIFIED	22. Price